NASA Technical Paper 1507

A Critical Examination of Stresses in an Elastic Single Lap Joint

Paul A. Cooper and James Wayne Sawyer

SEPTEMBER 1979

NASA

NASA Technical Paper 1507

A Critical Examination of Stresses in an Elastic Single Lap Joint

Paul A. Cooper and James Wayne Sawyer
Langley Research Center
Hampton, Virginia

National Aeronautics
and Space Administration

**Scientific and Technical
Information Branch**

1979

SUMMARY

The results of an approximate nonlinear finite-element analysis of a single lap joint are presented and compared with the results of a linear finite-element analysis, and the geometric nonlinear effects caused by the load-path eccentricity on the adhesive stress distributions are determined. The approximate nonlinear finite-element solution is evaluated by comparison with a nonlinear solution obtained from a finite-difference analysis, and results are compared with the classical approximate analysis by Goland and Reissner. An experimental photoelastic study of the moment distribution in the lap-joint adherend is used to evaluate the adequacy of plate approximations for analyzing single lap joints. The results from finite-element, Goland-Reissner, and photoelastic analyses show that for a single lap joint the effect of the geometric nonlinear behavior of the joint has a sizable effect on the stresses in the adhesive. The Goland-Reissner analysis is sufficiently accurate in the prediction of stresses along the midsurface of the adhesive bond to be used for qualitative evaluation of the influence of geometric or material parametric variations. Detailed stress distributions in both the adherend and adhesive obtained from the finite-element analysis are presented to provide a basis for comparison with other solution techniques.

INTRODUCTION

Adhesively bonded joints offer the aerospace designer an attractive mass-efficient alternative to the mechanical fastening of structural components. (See, for example, ref. 1.) In the past, however, the poor reliability of bonded joints has in general dissuaded designers from taking full advantage of the projected benefits of bonded structural designs. Thus, growth in the use of bonded systems in load-carrying components is not keeping pace with the continuing development and improved reliability of new high-strength adhesives (refs. 1 and 2). Bonded joints should be designed to transfer load in shear with a minimum of peel across the bond line since adhesives are generally more efficient in supporting shear forces and perform poorly when supporting peel-type forces. Design of bonded joints thus requires knowledge of the shear and peel stress distributions in the bond line as well as the shear strength of the adhesive. The single lap joint (fig. 1) is the simplest joint which transfers in-plane load primarily by shear in the adhesive. In fact, the ASTM D 1002-72 single-lap-joint test (ref. 3) is the most popular experimental procedure for evaluating the shear strength of adhesives.

Application of an in-plane tensile load to the single lap joint causes the adherends to deform due to eccentricity in the load path. The deformations that result are of the order of the thickness of the adherend and an order of magnitude larger than the thickness of the bond line. As loading progresses, the internal moment at the edge of the overlap region is reduced considerably due to the deformation of the adherends. Since the moment directly influences the

shear and peel stress distributions in the adhesive, nonlinear solution procedures which reflect this reduction in moment may be necessary for accurate determination of these stresses.

A classic approximate analysis of single lap joints that takes into account the nonlinear action of the lap joint due to flexure of the adherends was published in 1944 (ref. 4) and is hereafter referred to as the Goland-Reissner solution. This analysis established the basis for the study of the stress distributions in single lap joints. The analysis was based on several assumptions, the most constraining being the assumption that the shear and peel stresses are both constant through the adhesive thickness. The assumption of constant shear stress leads to a nonvanishing adhesive shear stress at the free edge of the adhesive. The desire to remove these assumptions and to include other considerations, such as adhesive plasticity and adherend transverse shear deformation, prompted several researchers to refine the analysis (refs. 5 to 14). These refined analyses are based on fundamental plane strain elasticity approaches which require some approximations to either the governing equations or the solution techniques.

By the midsixties, researchers were approaching the problem using finite-element analyses. Most of the investigations were linear and used mesh sizes that were too coarse to adequately predict the adhesive shear-stress behavior near the free edge (refs. 15 to 20). One linear investigation did use a fine mesh to determine the free-edge conditions in the lap region (ref. 21). Several investigations were conducted using a nonlinear finite-element solution procedure to determine the stress distributions in the plastic range of the adhesive material (refs. 22 to 24) but did not consider the geometric nonlinear behavior.

The main purpose of this paper is to investigate the effect of geometric nonlinearity on the elastic stress distributions for single lap joints. First, the Goland-Reissner solution with slight modifications to the governing equations is compared with the same solution with the nonlinear terms suppressed. Next, an approximate nonlinear finite-element solution is obtained and its accuracy confirmed by comparison with a solution from an established nonlinear-analysis computer program which uses a finite-difference solution technique. These solutions are also compared with corresponding linear solutions to indicate the influence of the nonlinear terms. The finite-element solution is compared with the solution obtained from the Goland-Reissner analytical approach to investigate the limitations of this latter approach. Finally, detailed distributions through the adherend and adhesive obtained from the nonlinear finite-element solution are presented to provide a detailed picture of the stress behavior in a single lap joint loaded in the elastic range. The stresses thus obtained are examined to evaluate the appropriateness of the single-lap-joint configuration as a test specimen for the determination of adhesive shear strength.

Certain commercial materials are identified in this paper in order to specify adequately which materials were investigated in the research effort. In no case does such identification imply recommendation or endorsement of the product by NASA, nor does it imply that the materials are necessarily the only ones or the best ones available for the purpose.

SYMBOLS

A	extensional stiffness of adherend defined after equation (A3)
a	cross-sectional area of adherend
c	one-half overlap length
D	plate stiffness of adherend defined after equation (A2)
E	Young's modulus
G	shear modulus
I	centroidal moment of inertia of cross section of photoelastic adherend
k,k'	constants defined after equations (A8) and (A11), respectively
ℓ	length of adherend from point of load application to beginning of overlap
M	adherend moment resultant
$(M_o)_\ell$	adherend moment resultant at edge of overlap for stiff adhesive model based on linear analysis (see fig. 30)
P	applied load on photoelastic model
r_1,r_2	constants defined after equation (A11)
T	adherend load resultant, force per unit width
t	adherend thickness
u	adhesive displacement in direction normal to plane of adhesive
u_1,u_2	constants defined after equation (A15)
V	adherend transverse shear-force resultant
w	lateral displacement of adherend
x,y	lineal measure defined where used
Δ	constant defined after equation (A11)
δ	constant defined after equation (A6)
ε_x	adherend strain in longitudinal direction
ζ	ratio of adhesive to adherend thickness

η adhesive thickness

λ coefficient defined after equation (A11)

ν Poisson's ratio of adherend material

σ adhesive peel stress

σ_x normal stress in x-direction

σ_y normal stress in adherend in y-direction

τ adhesive shear stress

ϕ angular measure between line of axis of applied force and plane of bond

Subscripts:

a adhesive

app applied

av average

L lower adherend

max maximum

U upper adherend

o adherend stress resultant at edge of overlap

Whenever terms in appendix A differ from corresponding terms in reference 4, these terms are underlined with a dashed line.

GOLAND-REISSNER ANALYTICAL SOLUTION

Lap-Joint Configuration

The single-lap-joint configuration used throughout this study is based on the ASTM D 1002-72 test specimen used to obtain strength properties of adhesives in shear by tension loading. The dimensions of the joint are given in figure 1; the material properties assumed for this study are given in table I and are based on a titanium adherend and an aluminum-filled polyimide adhesive. The adherend thickness used in this study is slightly less than that suggested by ASTM D 1002-72.

Adhesive Stress Distribution

The classical approximate analysis of reference 4 for a single lap joint with a flexible adhesive is repeated in appendix A with some slight modifications to improve the consistency of the analysis. The shear distribution τ and the peel stress (stress normal to the plane of the bond) σ in the adhesive along the bond line are given by

$$\frac{\tau}{\tau_{av}} = \frac{1}{4 + 3\zeta}\left[(1 + 3k)\frac{\delta}{\sinh \delta}\cosh\left(\frac{\delta x}{c}\right) + 3(1 - k + \zeta)\right] \tag{A8}$$

and

$$\frac{\sigma}{\sigma_{app}} = \left(\frac{t}{c}\right)^2 \frac{1}{\Delta}\left[\left(\frac{r_1\lambda^2 k}{2} + k'\lambda \sinh \lambda \sin \lambda\right)\sinh\left(\frac{\lambda x}{c}\right)\sin\left(\frac{\lambda x}{c}\right)\right.$$

$$\left. + \left(\frac{r_2\lambda^2 k}{2} + k'\lambda \cosh \lambda \cos \lambda\right)\cosh\left(\frac{\lambda x}{c}\right)\cos\left(\frac{\lambda x}{c}\right)\right] \tag{A11}$$

where all quantities are defined in appendix A. The constants k and k' are linearly related to the applied load.

In the derivation of these equations, several assumptions are made. The adhesive shear and peel stresses are assumed to be constant through the adhesive thickness, and the adhesive direct stress parallel to the adherends is assumed negligible. The adherend and adhesive materials are assumed to be elastic and to behave linearly. The shear deformations in the adherends and the influence of the adhesive on the flexural stiffness of the joint are assumed negligible, and the adherends are assumed to deform as a plate in cylindrical bending.

As a result of these approximations, an adhesive free-edge boundary condition, $\tau = 0$, is unsatisfied. Concern with the nonvanishing shear stress at the edge of the adhesive is probably unjustified since real lap joints often have adhesive runout at the overlap edges. Although this adhesive runout is probably of lesser strength and stiffness than the adhesive in the overlap region, which is cured under pressure, it can support shear stress. An analysis of the shear stress distribution in an adhesive fillet at the edge of the lap is studied in reference 21. The authors assumed that the adhesive fillet material had the same properties as the adhesive in the bond line.

Adherend Moment Distribution

The transverse deformations of the adherend are shown in figure 2 for two load levels. In a linear analysis, these deformations would be ignored in computing the moment distribution along the adherend. When accounted for in the calculation of the moment, these deformations can reduce the moment considerably from that calculated by assuming no relieving deformation, as shown in figure 3. The moment distribution is obtained by using a plate theory approximation, the accuracy of which is questionable in the vicinity of the overlap because of large transverse normal stresses and shear stresses which exist in this region. In order to investigate the accuracy of this approximation, a photoelastic study of a series of lap joints was performed and is presented in appendix B. The photoelastic study showed that the approximation for the moment distribution in the adherend is better for lap joints when the adhesive is flexible compared with the adherend than when the adhesive has the same stiffness as the adherend. The results of the study indicate that the adherend does have a stress distribution consistent with that of a cylindrically bent plate, even near the overlap region.

Comparison of Linear and Nonlinear Stress Distributions

The computed adhesive nondimensional shear and peel stress distributions along the bond line are shown in figures 4 and 5, respectively, for applied loads in the working range for common adhesives and for the linear solution which gives stress concentrations independent of load level. The computed stress concentrations at the edge of the lap $\left(\frac{x}{c} = 0\right)$ are reduced for both the shear and peel stresses as the applied load increases and are considerably below the stress concentrations predicted by linear solution. Differences in adhesive stresses are less severe at points in the interior of the lap region. The stress concentrations are plotted as a function of applied load in figure 6. The linear solution gives the maximum values of the stress concentrations and represents the limiting case for an infinitesimal applied load. The stress concentrations computed with the nonlinear terms retained drop appreciably as the applied load increases from zero and then drop more slowly as the load increases further.

As the overlap length increases, the difference between the linear and nonlinear analyses increases rapidly; and as shown in figures 7 and 8, the linear analysis predicts stress concentrations considerably higher than those predicted by the nonlinear analysis. Several authors have investigated the accuracy of the Goland-Reissner nonlinear analysis with finite-element studies (refs. 15, 17, 21, and 22). In each instance the studies were made neglecting the nonlinear effects.

NUMERICAL ANALYSES

As discussed in the previous section, the Goland-Reissner analysis makes several simplifying assumptions. Finite-element and finite-difference analysis

computer codes that can more realistically model the physical conditions are available and have been used to analyze the ASTM D 1002-72 single lap joint. this section, a quasi-nonlinear finite-element solution of the lap joint is developed, compared with a nonlinear finite-difference solution to confirm its accuracy, and is then used to indicate the importance of the nonlinear influence. All numerical calculations were conducted for a specimen with the dimensions shown in figure 1.

Nonlinear Finite-Element Analysis

The finite-element program SPAR described in reference 25 was used to analyze the single lap joint. SPAR is intended to be used primarily to perform structural analyses of linear problems. The major motivation for using the SPAR program was its capability to efficiently handle large problems with a minimum of execution time, central memory, and secondary data storage requirements. These characteristics are particularly advantageous for the reanalysis procedures required in the nonlinear-analysis approach.

The finite-element mesh used to analyze the single lap joint is shown in figure 9(a). A total of 702 nodes and 624 triangular and quadrilateral membrane elements are used in the analysis. The element formulation was based on an assumed stress field with a minimum complementary energy method. (See ref. 26.) A similar analysis for a model with a smaller number of elements (496) gave results only slightly different from the present model, thus indicating that the modeling used is adequate. A very fine mesh was used in the critical areas where large stress gradients are expected, such as at the end of the adhesive and in the surrounding adherends. (See enlarged detail, fig. 9(a).) The adherend and adhesive thicknesses were each divided into five equal layers. In high stress gradient areas, the aspect ratios of the elements were always maintained between 1.0 and 3.0 to assure the accuracy of the analysis.

The closed-form analysis showed the importance of accounting for the bending moment in the joint due not only to the eccentricity of the loading but also to the deformation of the adherends as the load is applied. This interdependence of the bending moment, load, and deformation makes the problem geometrically nonlinear. Since the SPAR program is linear, an approximation to the nonlinear behavior is computed using SPAR by first obtaining a linear solution with the bending moment based on the undeformed shape. The initial stress-stiffness matrix associated with the applied load and the resulting deformations is calculated and then added to the initial stiffness matrix. Next, the linear SPAR analysis is rerun with the modified stiffness matrix to give a one-step approximation to the nonlinear problem. This process is repeated until convergence of the solution is achieved. It was found that only one recomputation was required to obtain convergence for the lap-joint analysis under consideration.

Nonlinear Finite-Difference Analysis

In order to verify the accuracy of the nonlinear finite-element approach, the single lap joint was analyzed by using the nonlinear finite-difference code STAGS described in reference 27. STAGS was developed primarily for the non-

linear analysis of shell or plate structures and includes geometric as well as material nonlinearity.

The finite-difference mesh used to analyze the single lap joint is shown in figure 9(b). Analyses using different mesh sizes indicated that a total of 1019 finite-difference stations were adequate to give converged results. Finite-difference nodes were concentrated in the critical areas where large stress gradients occur, such as at the end of the adhesive and in the surrounding adherends. (See enlarged detail in fig. 9(b).)

Comparison of Numerical Results

The results of the finite-element and finite-difference analyses for nondimensional shear and peel stress distributions along the center line of the adhesive are shown in figures 10 and 11. Both linear and nonlinear results are presented. The solid and dashed curves were obtained with the finite-element and finite-difference analyses, respectively. The two analyses agree well, especially in the critical region near the free edge of the adhesive shown by the expanded scale.

A comparison between the linear and nonlinear results shows that for a single lap joint the change in bending moment due to the lateral deflection of adherends should be taken into account. The maximum shear stresses along the center of the bond line in figure 10 differed by 28 percent, and the maximum peel stresses in figure 11 differed by 35 percent.

COMPARISON OF GOLAND-REISSNER AND FINITE-ELEMENT RESULTS

In figures 12 and 13, the shear and peel stresses for 175 kN/m (1000 lbf/in.) applied load obtained with the Goland-Reissner analysis taken from figures 4 and 5 are compared with the stress distributions along the midplane of the adhesive computed using both the linear and nonlinear finite-element procedures. Because of the high stiffness of the adhesive used in the current study, the lap-joint configuration under consideration is outside the suggested range of applicablity of the Goland-Reissner analysis as stated in reference 4 and slightly outside the relaxed range of applicability suggested in reference 28. However, with the exception of a small region near the overlap edge, agreement is excellent. The Goland-Reissner analysis is quite accurate in predicting the shear stress distribution at the center line of the adhesive over at least 95 percent of the bond line.

As seen in figure 12, the maximum shear stress concentrations computed by the nonlinear analyses differ by 12 percent, with the Goland-Reissner analysis giving the higher value. Both of these maximum values are considerably below the maximum shear stresses predicted by the corresponding linear analyses. The free-edge effect is shown in the figure and is restricted to a region within 2 percent of the overlap length.

As seen in figure 13, the maximum peel stress concentrations predicted by the Goland-Reissner and finite-element nonlinear analyses differ by approxi-

mately 25 percent, the Goland-Reissner analysis giving the higher value. The Goland-Reissner analysis is less accurate throughout a larger part of the overlap region in the prediction of the peel stress distribution than for the prediction of the shear stress distribution, but still gives good results over approximately 70 percent of the bond line.

As seen from these comparisons, the lack of satisfaction of the adhesive free-edge boundary condition in the Goland-Reissner analysis has a minor effect in the prediction of the adhesive stress distributions along the center line of the adhesive except near the overlap edge. The form of the stress distributions and the prediction of the stress level are sufficiently accurate for determination of the qualitative behavior of single lap joints. Thus, the stress equations (A8) and (A11) provide an efficient procedure for a qualitative evaluation of the influence of different geometries and material properties on the center-line adhesive stresses.

The Goland-Reissner analysis assumes that the adhesive shear and peel stresses are constant through the thickness and neglects the in-plane direct stress. The shear, peel, and in-plane direct stress distributions at three locations through the adhesive thickness are plotted along the bond line in figures 14 to 16 and are compared with the results from the Goland-Reissner analysis. Over most of the bond line the shear and peel stresses show very little variation through the thickness. However, there is considerable variation through the thickness near the free edge of the adhesive due to the influence of the free-edge boundary condition and proximity to the reentrant corner. The direct stress in the adhesive is of the order of 10 percent of the applied adherend normal stress along most of the overlap but increases considerably in the vicinity of the free edge.

LAP-JOINT DETAILED STRESS DISTRIBUTIONS

Detailed stress distributions presented in the following sections can be used for comparison with other solution techniques and analyses. Stress distributions are presented through the thickness and along the length of both the adhesive and the adherend in figures 14 to 23. Since the finite-element analysis is an elastic analysis, a stress singularity exists at the reentrant corner where the free edge of the adhesive joins the adherend. The localized nature of the singular point is most evident in the stress distributions of the adhesive in figures 15 and 18 and in the adherend in figures 22 and 23. A further refinement of the finite-element modeling of the adherend and adhesive in the vicinity of the reentrant corner was made; and, although the maximum computed stress values increased rapidly as the singular point was approached, the values presented in the figures are at a sufficient distance from the singularity to remain unchanged. Although the stress data are presented in nondimensional form, it must be realized that the stresses vary nonlinearly with applied load and were calculated using a tensile load T of 175 kN/m (1000 lbf/in.) applied to a lap joint with dimensions given in figure 1. Use of nondimensional stress values for other load levels or other specimens would not be correct, as can be seen from figures 4, 5, 7, and 8.

Nondimensional stress distributions in the adhesive are presented in figures 14 to 19. Shear, peel, and in-plane stress distributions along the length of the adhesive at different positions through the thickness are shown in figures 14, 15, and 16, respectively. Shear, peel, and in-plane stress distributions across the adhesive thickness at several different positions along the joint length are shown in figures 17, 18, and 19, respectively.

Nondimensional transverse and axial stress distributions in the adherend are shown in figures 20 to 23. Figures 20 and 21 show the transverse and axial stress distributions through the adherend thickness at various positions along the adherend, and figures 22 and 23 show the stress distributions along the adherend at various positions through the thickness. The transverse normal stresses (figs. 20 and 22) in the adherend are near zero except near the free edge of the adhesive where large values and variations occur both along and across the adherend. The large transverse tensile stresses and gradients prove especially detrimental for filamentary composite single lap joints due to the low interlaminar strength of most composite laminates.

The axial stresses vary linearly through the adherend thickness (fig. 21) except at the edge of the overlap. Near the center of the joint ($x/\ell = 0$, fig. 23), the axial stresses are approximately constant through the adherend thickness and are approximately 50 percent of the average applied stresses. Near the applied load, the axial-stress variation through the adherend thickness is small, and the stress values are approaching the average applied stresses. Along the adherend, the variations in the axial stress through the adherend thickness become larger near the overlap edge, thus reflecting the distribution in bending-moment trend shown in figure 3.

CRITIQUE OF ASTM D 1002-72 ADHESIVE SHEAR-STRENGTH TEST

Since the shear strength of an adhesive must be known before a joint design can be made, a practical inexpensive test procedure to evaluate the shear strength is desirable. The analyses performed in this paper are concerned with a lap-joint configuration similar to that suggested by ASTM D 1002-72, which is the most popular procedure for the evaluation of the shear strength of adhesive systems. The results suggest, in agreement with findings of others (refs. 19 and 21), that this test is inadequate even in a qualitative sense. A test specimen using an adhesive weak in peel strength but with high shear strength could fail at a load below that required to fail a test specimen bonded with an adhesive strong in peel strength but weak in shear strength. Thus, the evaluator could be led to an erroneous conclusion as to the relative shear strengths of the two adhesives. It appears that other established test techniques (ASTM E 229-70 or the thick-adherend test given in ref. 29), although lacking the simplicity and economy of the ASTM D 1002-72 test, should be used for evaluating adhesives or consideration should be given to the development of a simple economical test specimen which can replace the ASTM D 1002-72 specimen.

CONCLUDING REMARKS

A linear elastic finite-element analysis of a bonded single lap joint is modified to account for the nonlinear behavior of the joint due to the eccentricity of the load path. The influence of the nonlinear behavior on the stress distribution in the adhesive and adherend is sufficiently large so that a sizable error in the prediction of the adhesive shear and peel stress distributions can occur if the nonlinear effects are not included. This nonlinear behavior was shown experimentally in a photoelastic study of the single-lap-joint adherend.

Results from the classic closed-form approximate analysis of Goland and Reissner for an elastic single lap joint, which does take into account the flexibility of the adherends and joint rotation, are compared with the finite-element solution for a lap-joint configuration similar to the ASTM D 1002-72 standard test specimen for evaluation of the shear strength of adhesives. Results from this comparison indicate that the Goland-Reissner solution is sufficiently accurate to be used in the qualitative prediction of the influence of parametric variations on the shear and peel stresses along the center of the adhesive bond line. The closed-form solution does not satisfy the adhesive free-edge shear boundary condition, but the influence of the free edge is confined to a small zone and has little influence on the computed maximum value of the shear or peel stress occurring along the center of the adhesive bond line. Inspection of the adhesive stress distribution obtained with a finite-element analysis shows that the assumption of constant shear and peel stress through the adhesive thickness used in the Goland-Reissner solution is valid over the interior of the lap region but deteriorates in the vicinity of the free-edge reentrant corner where a two-dimensional elastic analysis predicts singular stresses.

The method of evaluating the internal moment in the adherend used in the Goland-Reissner approach, which assumes that the joint deforms as a plate in cylindrical bending, is shown by both the finite-element results and a photoelastic study to be accurate even near the region of the overlap for an adhesive with a modulus much less than the modulus of the adherend.

Detailed stress distributions at several locations in both the adherend and adhesive are presented to provide a basis for comparison with other solution techniques. Inspection of the stress distribution in the ASTM D 1002-72 lap-joint configuration shows that this test specimen is inadequate for determining the shear strength of adhesives even in a qualitative sense.

Langley Research Center
National Aeronautics and Space Administration
Hampton, VA 23665
July 27, 1979

APPENDIX A

DERIVATION OF GOLAND-REISSNER EQUATIONS FOR ADHESIVE SHEAR AND PEEL STRESS

The development of the shear and peel stress equations is similar to that of reference 4, but with plate behavior being assumed consistent throughout the development and, in addition, small terms formerly ignored being retained for completeness. Wherever terms differ from corresponding terms in reference 4, these terms are underlined with a dashed line.

The sign convention used throughout this analysis is shown in figure 24. A differential element of a slice through the bonded region is shown in figure 25 where the adhesive is assumed to act as a spring with both shear and transverse extensional stiffness so that stress is assumed constant through the thickness. The integrated internal stresses (stress resultants) are applied on the vertical cut, thus reducing the analysis to a one-dimensional plane-strain analysis.

From equilibrium considerations,

$$\frac{dT_U}{dx} + \tau = 0 \tag{A1a}$$

$$\frac{dT_L}{dx} - \tau = 0 \tag{A1b}$$

$$\frac{dM_U}{dx} - V_U + \underline{\tau\left(\frac{\eta + t}{2}\right)} = 0 \tag{A1c}$$

$$\frac{dM_L}{dx} - V_L + \underline{\tau\left(\frac{\eta + t}{2}\right)} = 0 \tag{A1d}$$

$$\frac{dV_U}{dx} + \sigma = 0 \tag{A1e}$$

$$\frac{dV_L}{dx} - \sigma = 0 \tag{A1f}$$

where the subscripts U and L refer to quantities in the upper and lower adherends of figure 25.

The assumption of plane strain leads to the load-displacement relationships of cylindrically bent plate theory

$$\frac{d^2 w_U}{dx^2} = -\frac{M_U}{D} \tag{A2a}$$

$$\frac{d^2 w_L}{dx^2} = -\frac{M_L}{D} \tag{A2b}$$

where the flexural stiffness of the adherend is given by

$$D = \frac{Et^3}{12(1 - \nu^2)}$$

The reduction of the flexural stiffness due to the existence of the adhesive bond line is ignored, and shear deformations in the adherend are neglected as being small compared with flexural deformations. The longitudinal strain at the adhesive-adherend interface due to flexure is given by

$$(\varepsilon_x)_U = \frac{t}{2}\frac{M_U}{D}$$

$$(\varepsilon_x)_L = -\frac{t}{2}\frac{M_L}{D}$$

so that the total strain in terms of forces and moments becomes

$$\frac{du_U}{dx} = \frac{T_U}{A} + \frac{t}{2}\frac{M_U}{D} \tag{A3a}$$

$$\frac{du_L}{dx} = \frac{T_L}{A} - \frac{t}{2}\frac{M_L}{D} \tag{A3b}$$

where

$$A = \frac{Et}{1 - \nu^2}$$

Since the adhesive shear and transverse normal stresses are assumed constant through the adhesive thickness, then

$$\tau = G_a\left(\frac{u_L - u_U}{\eta}\right) \tag{A4a}$$

$$\sigma = E_a\left(\frac{w_L - w_U}{\eta}\right) \tag{A4b}$$

If only the overlap region is considered, the stress resultant continuity conditions can be given as

$$\left.\begin{aligned} &V_L = M_L = T_L = 0 \\ &V_U = V_o;\quad M_U = M_o;\quad T_U = T_o \end{aligned}\right\} \qquad (x = -c) \tag{A5a}$$

$$\left.\begin{aligned} &V_U = M_U = T_U = 0 \\ &V_L = V_o;\quad M_L = -M_o;\quad T_L = T_o \end{aligned}\right\} \qquad (x = c) \tag{A5b}$$

where quantities with subscript o are the internal stress resultants applied by the adjoining adherends.

Differentiating equation (A4a) twice and equations (A3) once, combining the resultant equations to remove u_L and u_U, and substituting for the derivatives of M and T by using equations (A1a) to (A1d) result in the following equation:

$$\frac{d^2\tau}{dx^2} = \frac{G_a}{\eta}\left\{2\tau_o\left[\frac{1}{A} + \frac{t}{2D}\left(\frac{\eta + t}{2}\right)\right] - \frac{t}{2D}(V_L + V_U)\right\}$$

On differentiating this equation once and using equations (A1e) and (A1f) to remove V, the equation governing the distribution of shear stress in the adhesive is found to be

$$\frac{d^3\tau}{dx^3} - \left(\frac{\delta}{c}\right)^2 \frac{d\tau}{dx} = 0 \tag{A6}$$

where

$$\delta^2 = \frac{8G_a(1 - \nu^2)}{\eta E t}\left(1 + \frac{3\zeta}{4}\right)c^2$$

and

$$\zeta = \frac{\eta}{t}$$

The equation is subject to the following boundary conditions found from equations (A3) to (A5) and equilibrium of an adherend in the lap region:

$$\frac{d\tau}{dx}(-c) = \frac{-G_a(1 - \nu^2)}{\eta E t}\left(T_o + \frac{6M_o}{t}\right) \tag{A7a}$$

$$\frac{d\tau}{dx}(c) = \frac{G_a(1 - \nu^2)}{\eta E t}\left(T_o + \frac{6M_o}{t}\right) \tag{A7b}$$

Additionally from equilibrium of external forces,

$$\int_{-c}^{+c} \tau \, dx = T_o \tag{A7c}$$

The solution of the system of equations (A6) and (A7) is

$$\frac{\tau}{\tau_{av}} = \frac{1}{4 + 3\underline{\zeta}}\left[(1 + 3k)\frac{\delta}{\sinh \delta}\cosh\left(\frac{\delta x}{c}\right) + 3(1 - k + \underline{\zeta})\right] \tag{A8}$$

where

$$\tau_{av} = \frac{T_o}{2c}$$

and

$$k = \frac{2M_o}{tT_o}$$

which reduces to the solution of reference 4 if $\zeta = 0$ and the term $1 - \nu^2$ is removed from the equation for δ^2.

Differentiating equation (A4b) three times, combining with equations (A2) differentiated once to remove w, and combining with equations (A1c) and (A1d) result in the following:

$$\frac{d^3\sigma}{dx^3} = \frac{E_a}{D\eta}(V_U - V_L)$$

On combining this equation with equations (A1e) and (A1f), the equation governing the peel stress in the adhesive is found to be

$$\frac{d^4\sigma}{dx^4} + \frac{2E_a}{D\eta}\sigma = 0 \tag{A9}$$

Equation (A9) is subject to the following boundary conditions found from equations (A2), (A4), and (A7):

$$\left.\frac{d^2\sigma}{dx^2}\right|_{-c} = \left.\frac{d^2\sigma}{dx^2}\right|_{c} = \frac{E_a}{\eta D} M_o \qquad \text{(A10a)}$$

$$\left.\frac{d^3\sigma}{dx^3}\right|_{-c} = -\left.\frac{d^3\sigma}{dx^3}\right|_{c} = \frac{E_a}{\eta D} V_o \qquad \text{(A10b)}$$

The solution of the system of equations (A9) and (A10) is

$$\frac{\sigma}{\sigma_{app}} = \left(\frac{t}{c}\right)^2 \frac{1}{\Delta}\left[\left(\frac{r_1\lambda^2 k}{2} + k'\lambda \sinh\lambda \sin\lambda\right)\sinh\left(\frac{\lambda x}{c}\right)\sin\left(\frac{\lambda x}{c}\right) + \left(\frac{r_2\lambda^2 k}{2} + k'\lambda \cosh\lambda \cos\lambda\right)\cosh\left(\frac{\lambda x}{c}\right)\cos\left(\frac{\lambda x}{c}\right)\right] \qquad \text{(A11)}$$

where

$$\sigma_{app} = \frac{T_o}{t}$$

$$\lambda = c\sqrt[4]{\frac{E_a}{2\eta D}}$$

$$\Delta = \frac{1}{2}(\sin 2\lambda + \sinh 2\lambda)$$

$$r_1 = \cosh\lambda \sin\lambda + \sinh\lambda \cos\lambda$$

$$r_2 = \sinh\lambda \cos\lambda - \cosh\lambda \sin\lambda$$

$$k' = \frac{cV_o}{tT_o}$$

APPENDIX A

The values of T_o, M_o, and V_o must be evaluated to complete the solution. To obtain approximations of these internal stress resultants, the lap joint is assumed to behave as a wide beam loaded in in-plane tension with a discontinuous neutral surface, as shown in figure 26. This assumption is of questionable accuracy near the lap region where its accuracy depends to a large degree on the relative flexibility of the adhesive. To examine this assumption, two photoelastic lap-joint models with stiff and flexible adhesives were analyzed. The results of this study are given in appendix B.

The cross-sectional moments in regions 1 and 2 can be given by

$$M_1 = T \cos\phi (x_1 \tan\phi - w_1)$$

$$M_2 = T \cos\phi \left[(x_2 - c) \tan\phi - w_2\right]$$

so that the beam equations governing the total lap-joint deformation can be given as

$$\frac{d^2w_1}{dx_1^2} = -\frac{T \cos\phi}{D}(x_1 \tan\phi - w_1) \qquad (0 < x_1 < \ell) \qquad \text{(A12a)}$$

$$\frac{d^2w_2}{dx_2^2} = -\frac{T \cos\phi}{8D}\left[(x_2 - c) \tan\phi - w_2\right] \qquad (0 < x_2 < c) \qquad \text{(A12b)}$$

subject to the boundary and continuity conditions

$$w_1|_0 = 0 \qquad \text{(A13a)}$$

$$w_2|_c = 0 \qquad \text{(A13b)}$$

$$w_1|_\ell = w_2|_0 \qquad \text{(A13c)}$$

$$\left.\frac{dw_1}{dx}\right|_\ell = \left.\frac{dw_2}{dx}\right|_0 \qquad \text{(A13d)}$$

The presence of terms containing the product of T and w make equations (A12) nonlinear with respect to the applied load. In addition, from geometric consid-

erations and simple plate theory, the stress resultants at the interface between the lap region and the single adherend can be given by:

$$T_o = T \cos \phi \tag{A14a}$$

$$M_o = -\frac{1}{D} \left. \frac{d^2 w_1}{dx_1^2} \right|_{\ell} \tag{A14b}$$

$$V_o = -\frac{1}{D} \left. \frac{d^3 w_1}{dx_1^3} \right|_{\ell} \tag{A14c}$$

Solution of the system of equations (A12) to (A14) yields

$$M_o = T\left(\frac{t + \eta}{2}\right) \cos \phi \, \frac{u_2 \cosh(u_2 c) \sinh(u_1 \ell)}{u_2 \sinh(u_1 \ell) \cosh(u_2 c) + u_1 \cosh(u_1 \ell) \sinh(u_2 c)} \tag{A15a}$$

$$V_o = T\left(\frac{t + \eta}{2}\right) \cos \phi \, \frac{u_1 u_2 \cosh(u_2 c) \cosh(u_1 \ell)}{u_2 \sinh(u_1 \ell) \cosh(u_2 c) + u_1 \cosh(u_1 \ell) \sinh(u_2 c)} \tag{A15b}$$

where

$$\cos \phi = \frac{\ell + c}{\sqrt{(\ell + c)^2 + \left(\frac{t + \eta}{2}\right)^2}}$$

$$u_1 = \sqrt{\frac{T \cos \phi}{D}}$$

$$u_2 = \sqrt{\frac{T \cos \phi}{8D}}$$

APPENDIX A

The solution of the stress resultants reduces to the values of T_o, M_o, and V_o of reference 4 for $\cos \phi = 1$.

If the adherends are assumed rigid so that D approaches infinity, the applied moment and shear distributions in the adherends reduce to

$$M_1 = T\left(\frac{t + \eta}{2}\right)\left(\frac{x_1}{\ell + c}\right) \cos \phi \tag{A16a}$$

$$V_1 = T\left(\frac{t + \eta}{2}\right)\left(\frac{1}{\ell + c}\right) \cos \phi \tag{A16b}$$

and the adhesive shear and peel stresses given by equations (A8) and (A11) are linearly related to the applied tensile-force resultant.

APPENDIX B

PHOTOELASTIC EXAMINATION OF LAP-JOINT ADHERENDS

Three photoelastic models shown in figure 27 were examined to evaluate the moment distribution in the adherend in the region outside the overlap for single lap joints with either stiff or flexible adhesives. The adherends of the models were fabricated from an epoxy material (PSM-5). The models were sized to approximate the geometric ratios of the ASTM D 1002-72 test specimen. Several photoelastic studies have been made previously of lap joints (refs. 20 and 30 to 32), but in each case the models considered had impractical geometrical ratios. The first model, shown in figure 28(a), is an integral model representative of a lap joint with an adhesive of the same material as the adherend. The second lap-joint model (fig. 28(b)) is an actual joint bonded with PMC-1 adhesive, which has properties similar to the adherend and cures at room temperature. This model has a stress-distribution pattern very similar to the integral model. The third model (fig. 28(c)) is a lap joint with a soft epoxy material (PS-3) bonded between the adherends to represent an adhesive with shear and extensional moduli well below the adherend moduli. The material properties and required stress optic constant for the PSM-5 photoelastic material are given in table II. All models were loaded to 133 N (30 lbf).

The experimental moments are determined by assuming that the adherend deforms as a simple beam subject to in-line tension so that the principal stresses determined from the isochromatic fringes are assumed directed along the axis of the adherend. Inspection of the isoclinics showed this assumption to be nearly correct everywhere in the adherend outside the overlap region for the model with the flexible adhesive and everywhere except close to the overlap in the integral and stiff adhesive models. The axial stresses are determined at several points across the adherend model width for each axial location. A best-fit straight line is computed using a least-squares procedure and the stress determined at one boundary by extrapolation. The results for three locations along the adherend in the integral model are shown in figure 29. The model with the stiff adhesive exhibited the same behavior as the integral model, as seen by comparison of the isochromatics shown in figures 28(a) and 28(b). The stress distributions are nearly linear across the width of the model at each location along the adherend except near the overlap region. For the model with the soft adhesive, the stress distributions are nearly linear at all locations outside the overlap region. The moment is computed from the approximate beam-rod equation

$$M_1 = -\frac{2I}{t}\left(\sigma_x\Big|_{y=0} - \frac{P}{a}\right)$$

where I is the moment of inertia of the cross section about the cross-sectional centroid, a is the area of the adherend cross section, σ_x is the extrapolated stress at the boundary, t is the width of the adherend (fig. 29), and P is the applied load. The evaluated moment distribution in the adherend

of each model near the overlap region is shown in figure 30 and is compared with the moment distribution calculated from the Goland-Reissner analysis for the stiff and flexible adhesive models.

The Goland-Reissner analysis neglects the adhesive in the computation of the moment and shear-force resultants in the adherend. As shown in figure 30, the agreement between the computed and experimentally determined moments for the flexible adhesive model is good everywhere in the adherend (within 9 percent). Thus, the error due to neglect of the bending stiffness of the adhesive in the computation of the moment is slight. The agreement is also good for the stiff adhesive models, except close to the lap edge where large transverse normal stresses and shear stresses begin to dominate - resulting in 15 percent error. Neglect of these stresses in the computation of the moment in the vicinity of the lap can lead to some error. Further, and perhaps more significant, a comparison of the experimental results with the moment calculated assuming a rigid adherend, which is the assumption tacitly made using a linear analysis, shows that the difference in moment due to the flexibility of the adherend is considerable and predicted well by the Goland-Reissner analysis. This comparison demonstrates experimentally the geometric nonlinear effect in the calculation of the adherend moment at the edge of the lap M_o.

REFERENCES

1. Thrall, Edward W., Jr.: Primary Adhesively Bonded Structure Technology (PABST). J. Aircr., vol. 14, no. 6, June 1977, pp. 588-594.

2. National Materials Advisory Board of the National Research Council: Structural Adhesives With Emphasis on Aerospace Applications. Volume 4 of Treatise on Adhesion and Adhesives, Robert L. Patrick, ed., Marcel Dekker, Inc., c.1976.

3. Standard Test Method for Strength Properties of Adhesives in Shear by Tension Loading (Metal-to-Metal). ASTM Designation: D 1002-72. Part 22 of 1978 Annual Book of ASTM Standards, c.1978, pp. 253-257.

4. Goland, M.; and Reissner, E.: The Stresses in Cemented Joints. J. Appl. Mech., vol. 11, no. 1, Mar. 1944, pp. A-17 - A-27.

5. Sherrer, R. E.: Stresses in a Lap Joint With Elastic Adhesive. Rep. No. 1864, Forest Products Lab., Forest Service, U.S. Department of Agriculture, Sept. 1957.

6. Corvelli, N.; and Saleme, E.: Analysis of Bonded Joints. Rep. No. ADR 02-01-70.1, Grumman Aerosp. Corp., July 1970.

7. Pahoja, Murlidhar H.: Stress Analysis of an Adhesive Lap Joint Subjected to Tension, Shear Force and Bending Moments. T. & A. M. Rep. No. 361 (Contract N00019-72-C-0274), Univ. of Illinois at Urbana, Aug. 1972. (Available from DDC as AD 753 469.)

8. Wah, Thein: Stress Distribution in a Bonded Anisotropic Lap Joint. Trans. ASME, Ser. H: J. Eng. Mater. & Technol., vol. 95, no. 3, July 1973, pp. 174-181.

9. Hart-Smith, L. J.: Adhesive-Bonded Single-Lap Joints. NASA CR-112236, 1973.

10. Pirvics, Juris: Two Dimensional Displacement-Stress Distributions in Adhesive Bonded Composite Structures. J. Adhes., vol. 6, no. 3, 1974, pp. 207-228.

11. Srinivas, S.: Analysis of Bonded Joints. NASA TN D-7855, 1975.

12. Allman, D. J.: A Theory for Elastic Stresses in Adhesive Bonded Lap Joints. Q. J. Mech. & Appl. Math., vol. 30, pt. 4, 1977, pp. 415-436.

13. Renton, W. J.; and Vinson, J. R.: Analysis of Adhesively Bonded Joints Between Panels of Composite Materials. J. Appl. Mech., vol. 44, ser. E, no. 1, Mar. 1977, pp. 101-106.

14. Ojalvo, I. U.; and Eidinoff, H. L.: Bond Thickness Effects Upon Stresses in Single-Lap Adhesive Joints. AIAA J., vol. 16, no. 3, Mar. 1978, pp. 204-211.

15. Kutscha, D.; and Hofer, K. E., Jr.: Feasibility of Joining Advanced Composite Flight Vehicle Structures. AFML-TR-68-391, U.S. Air Force, Jan. 1969. (Available from DDC as AD 690 616.)

16. Clark, G. A.; and Clayton, K. I.: Fabrication Techniques for Advanced Composite Attachments and Joints. AFML-TR-69-151, U.S. Air Force, May 1969. (Available from DDC as AD 859 506.)

17. Wooley, Gary R.; and Carver, Dale R.: Stress Concentration Factors for Bonded Lap Joints. J. Aircr., vol. 8, no. 10, Oct. 1971, pp. 817-820.

18. Barker, Richard M.; and Hatt, Fritz: Analysis of Bonded Joints in Vehicular Structures. AIAA J., vol. 11, no. 12, Dec. 1973, pp. 1650-1654.

19. Guess, T. R.; Allred, R. E.; and Gerstle, F. P., Jr.: Comparison of Lap Shear Test Specimens. J. Test. & Eval., vol. 5, no. 3, Mar. 1977, pp. 84-93.

20. Thongcharoen, V.: Optimization of Bonded Joints by Finite Element and Photoelasticity Methods. Ph. D. Thesis, Iowa State Univ. of Sci. & Technol., 1977.

21. Adams, R. D.; and Peppiatt, N. A.: Stress Analysis of Adhesive-Bonded Lap Joints. J. Strain Anal., vol, 9, no. 3, July 1974, pp. 185-196.

22. Grimes, G. C.; Greimann, L. F.; Wah, T.; Commerford, G. E.; Blackstone, W. R.; and Wolfe, G. K.: The Development of Nonlinear Analysis Methods for Bonded Joints in Advanced Filamentary Composite Structures. AFFDL-TR-72-97, U.S. Air Force, Sept. 1972. (Available from DDC as AD 905 201.)

23. Liu, An-Ton: Linear Elastic and Elasto-Plastic Stress Analysis for Adhesive Lap Joints. Ph. D. Thesis, Univ. of Illinois at Urbana-Champaign, 1976.

24. Humphreys, Edward A.; and Herakovich, Carl T.: Nonlinear Analysis of Bonded Joints With Thermal Effects. VPI-E-77-19 (NASA Grant NGR-47-004-090), Virginia Polytech. Inst. & State Univ., June 1977. (Available as NASA CR-153263.)

25. Whetstone, W. D.: SPAR Structural Analysis System Reference Manual - System Level 13A. Volume I: Program Execution. NASA CR-158970, 1978.

26. Pian, Theodore H. H.: Derivation of Element Stiffness Matrices by Assumed Stress Distributions. AIAA J., vol. 2, no. 7, July 1964, pp. 1333-1336.

27. Almroth, B. O.; and Brogan, F. A.: The STAGS Computer Code. NASA CR-2950, 1978.

28. Adams, R. D.; and Peppiatt, N. A.: Stress Analysis of Adhesive Bonded Tubular Lap Joints. J. Adhes., vol. 9, no. 1, 1977, pp. 1-18.

29. Renton, W. J.; and Vinson, J. R.: Shear Property Measurements of Adhesives in Composite Material Bonded Joints. Composite Reliability, ASTM STP 580, 1975, pp. 119-132.

30. Mylonas, C.: On the Stress Distribution in Glued Joints. Proceedings of the Seventh International Congress for Applied Mechanics, 1948, pp. 137-149.

31. McLaren, A. S.; and MacInnes, I.: The Influence on the Stress Distribution in an Adhesive Lap Joint of Bending of the Adhering Sheets. British J. Appl. Phys., vol. 9, Feb. 1958, pp. 72-77.

32. Tuzi, Ichiro; and Shimada, Heihachi: Photoelastic Investigation of the Stresses in Cemented Joints. Bull. JSME, vol. 7, no. 26, 1964, pp. 263-267.

TABLE I.- LAP-JOINT MATERIAL PROPERTIES

	Adherend	Adhesive
Young's modulus, GPa (psi)	110 (16×10^6)	17.9 (2.6×10^6)
Shear modulus, GPa (psi)	43. (6.2×10^6)	3.2 (0.46×10^6)
Poisson's ratio	0.3	0.19

TABLE II.- PHOTOELASTIC MATERIAL PROPERTIES

	PSM-5	PMC-1	PS-3
Young's modulus, GPa (psi)	3.1 (450×10^3)	2.9 (425×10^3)	0.21 (30×10^3)
Poisson's ratio	0.36	0.36	0.3
Fringe value, kPa-m per fringe (psi-in. per fringe)	10 (57.4)		

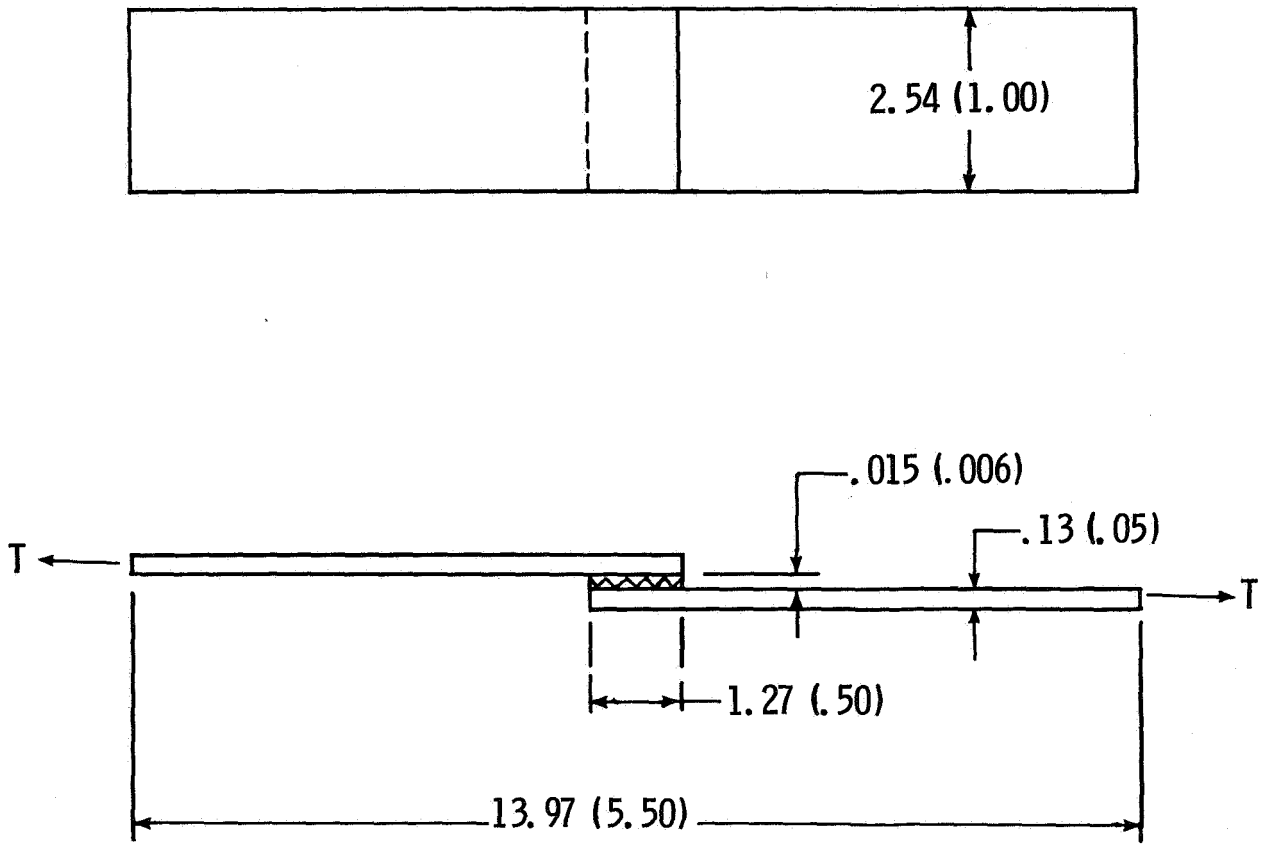

Figure 1.- Single-lap-joint geometry. Dimensions are given in centimeters (inches).

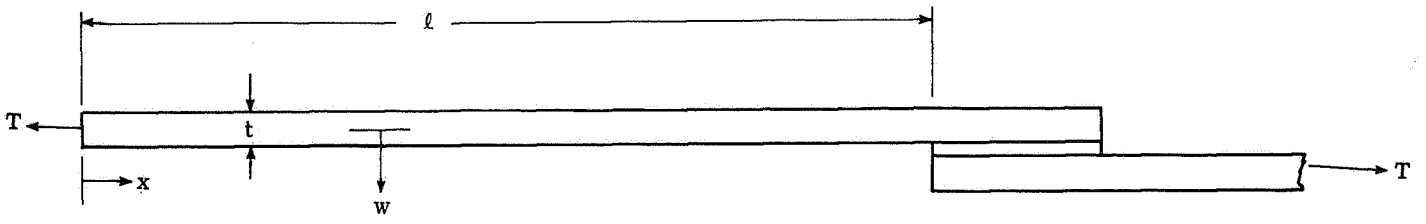

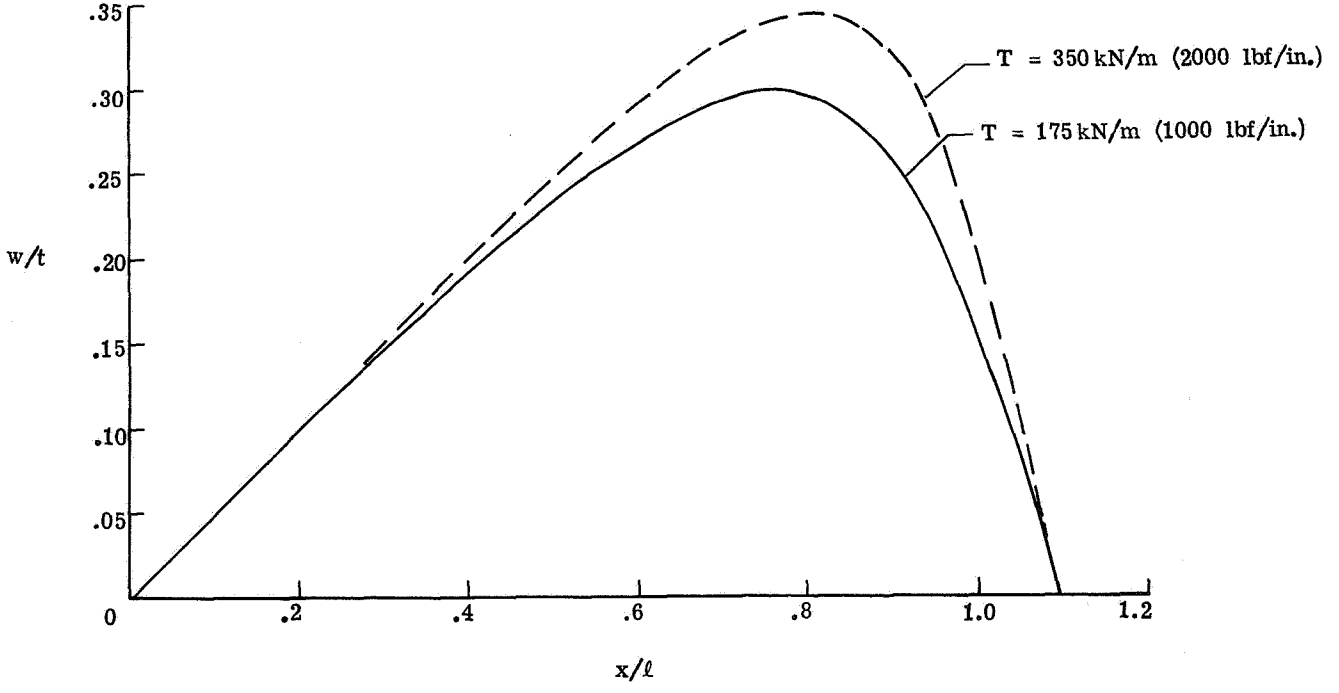

Figure 2.- Lap-joint displacement.

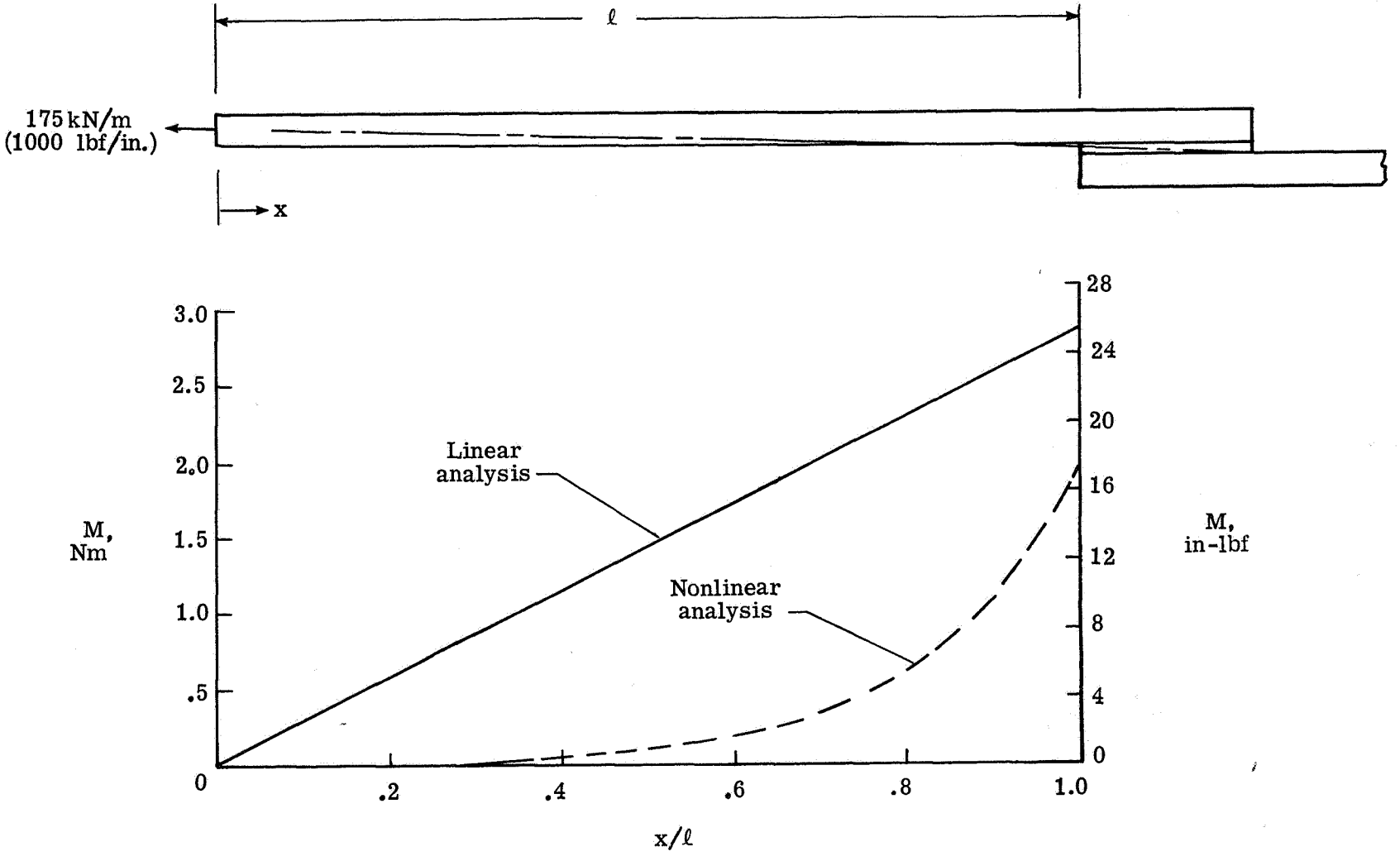

Figure 3.- Moment distribution in adherend.

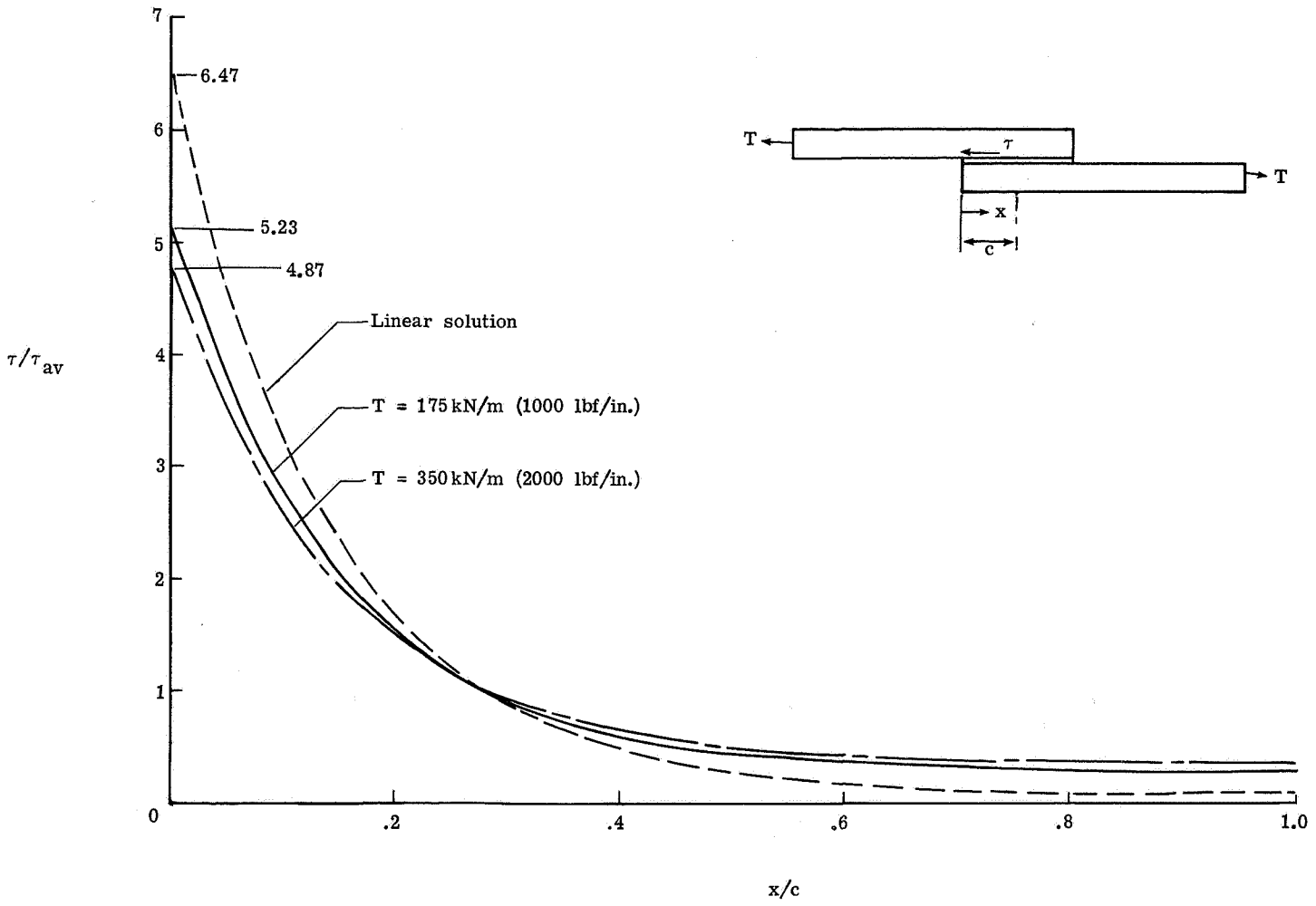

Figure 4.- Adhesive shear stress distribution at several load levels. Goland-Reissner analysis; c = 0.64 cm (0.25 in.); τ_{av} = T/2c.

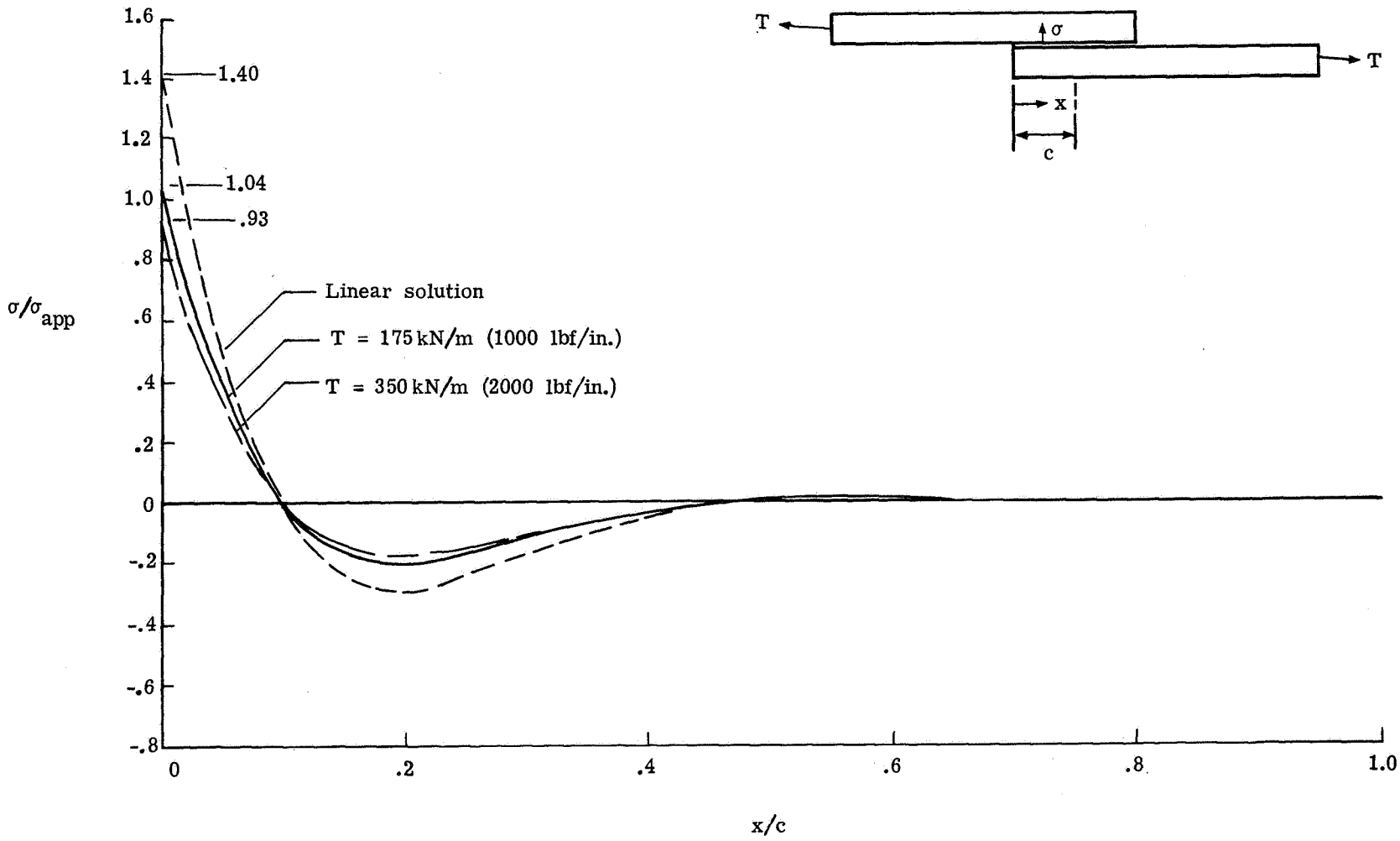

Figure 5.- Peel stress distributions for several load levels. Goland-Reissner analysis; c = 0.64 cm (0.25 in.); σ_{app} = T/t.

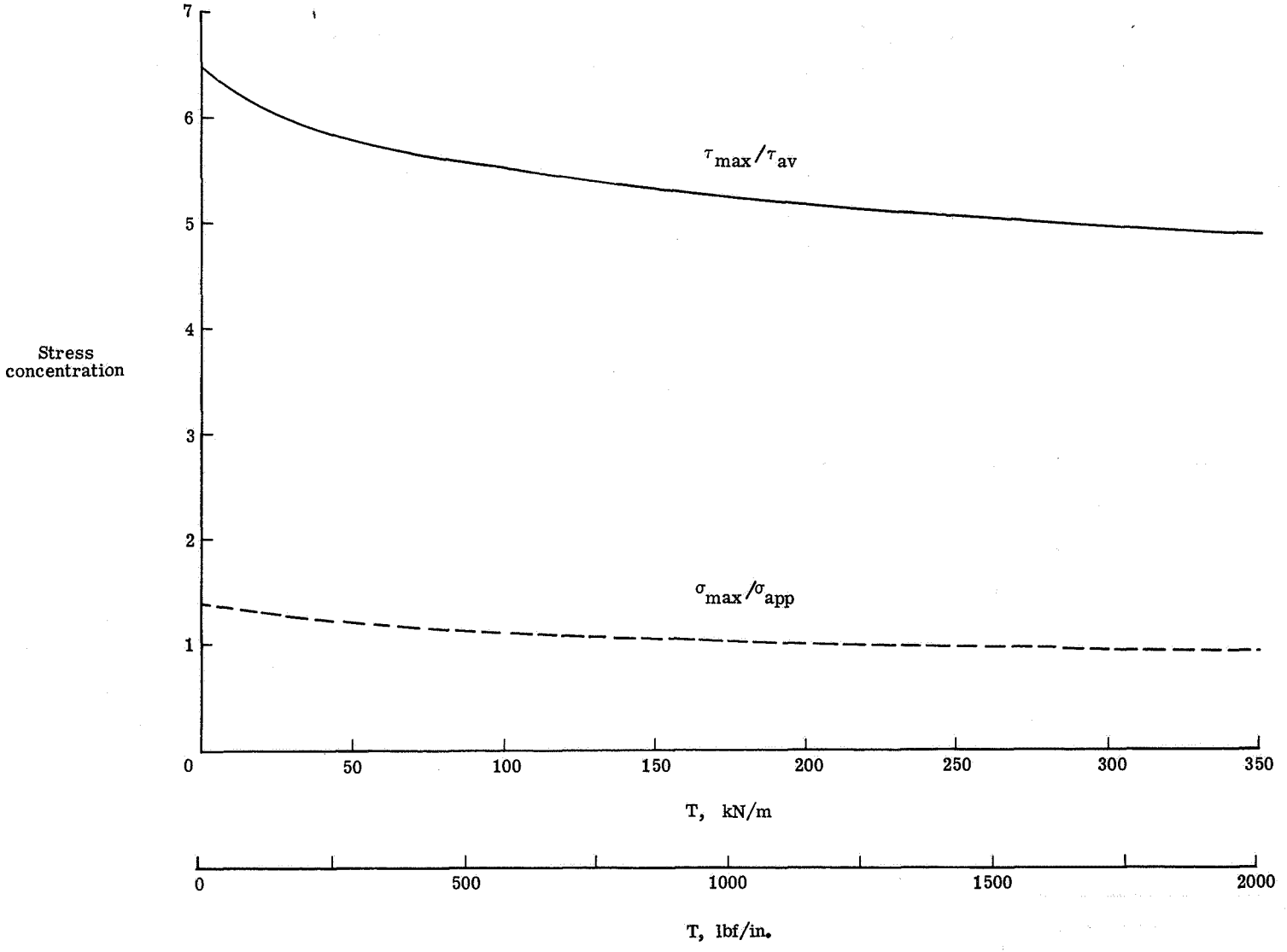

Figure 6.- Effect of applied load on maximum shear and peel stress concentrations in adhesive. Goland-Reissner analysis; c = 0.64 cm (0.25 in.); $\tau_{av} = T/2c$; $\sigma_{app} = T/t$.

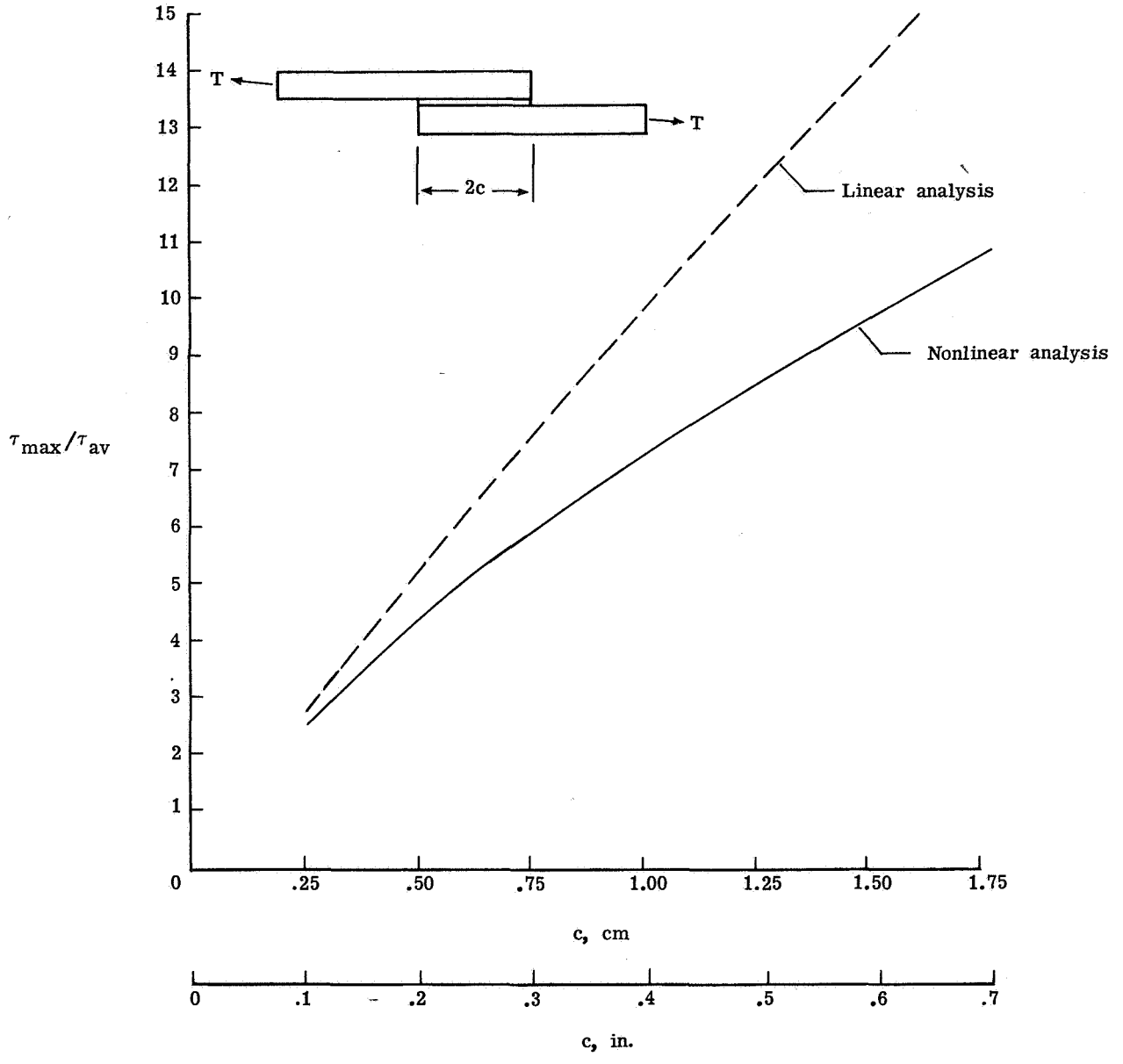

Figure 7.- Effect of joint overlap length on maximum shear stress in adhesive. Goland-Reissner analysis; T = 175 kN/m (1000 lbf/in.); τ_{av} = T/2c.

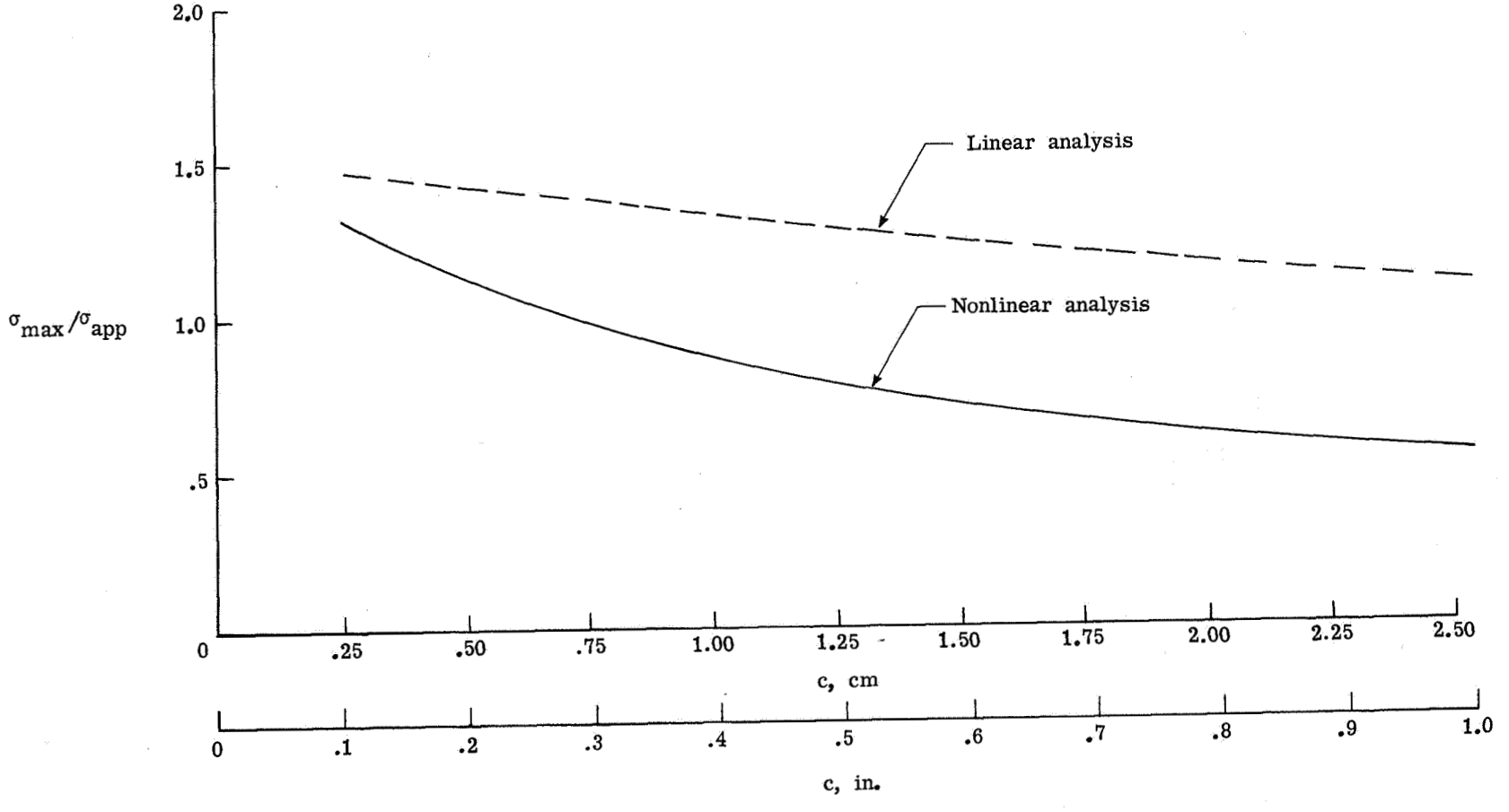

Figure 8.- Effect of joint overlap length on maximum peel stress in adhesive. Goland-Reissner analysis; T = 175 kN/m (1000 lbf/in.); $\sigma_{app} = T/t$.

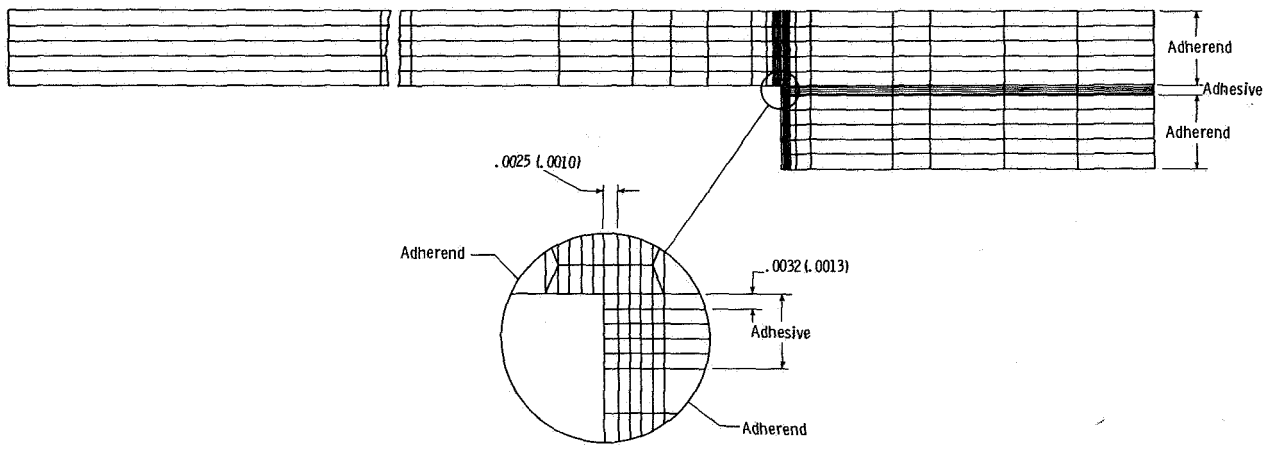

(a) SPAR (ref. 25) finite-element mesh.

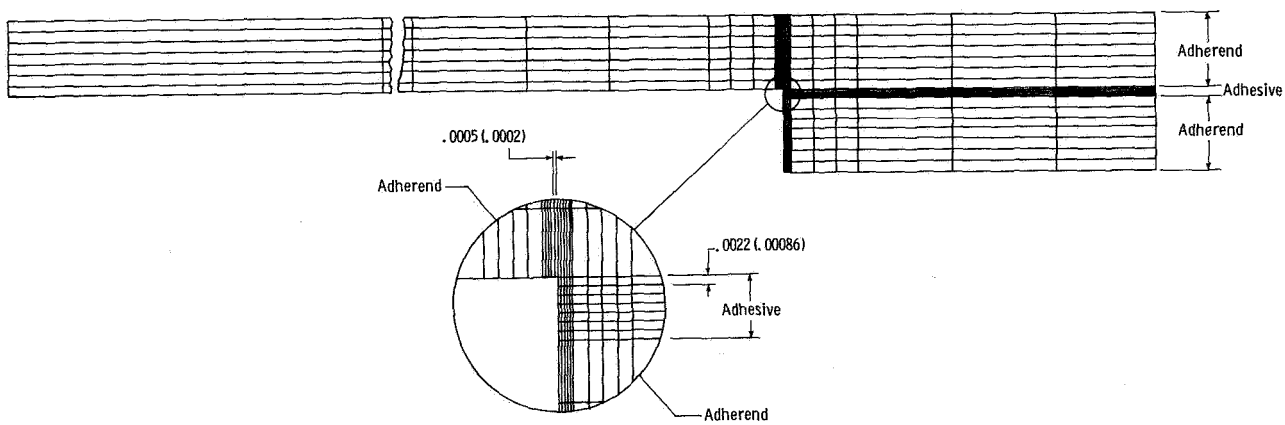

(b) STAGS (ref. 27) finite-difference mesh.

Figure 9.- Finite-element and finite-difference model of single lap joint. Dimensions are given in centimeters (inches).

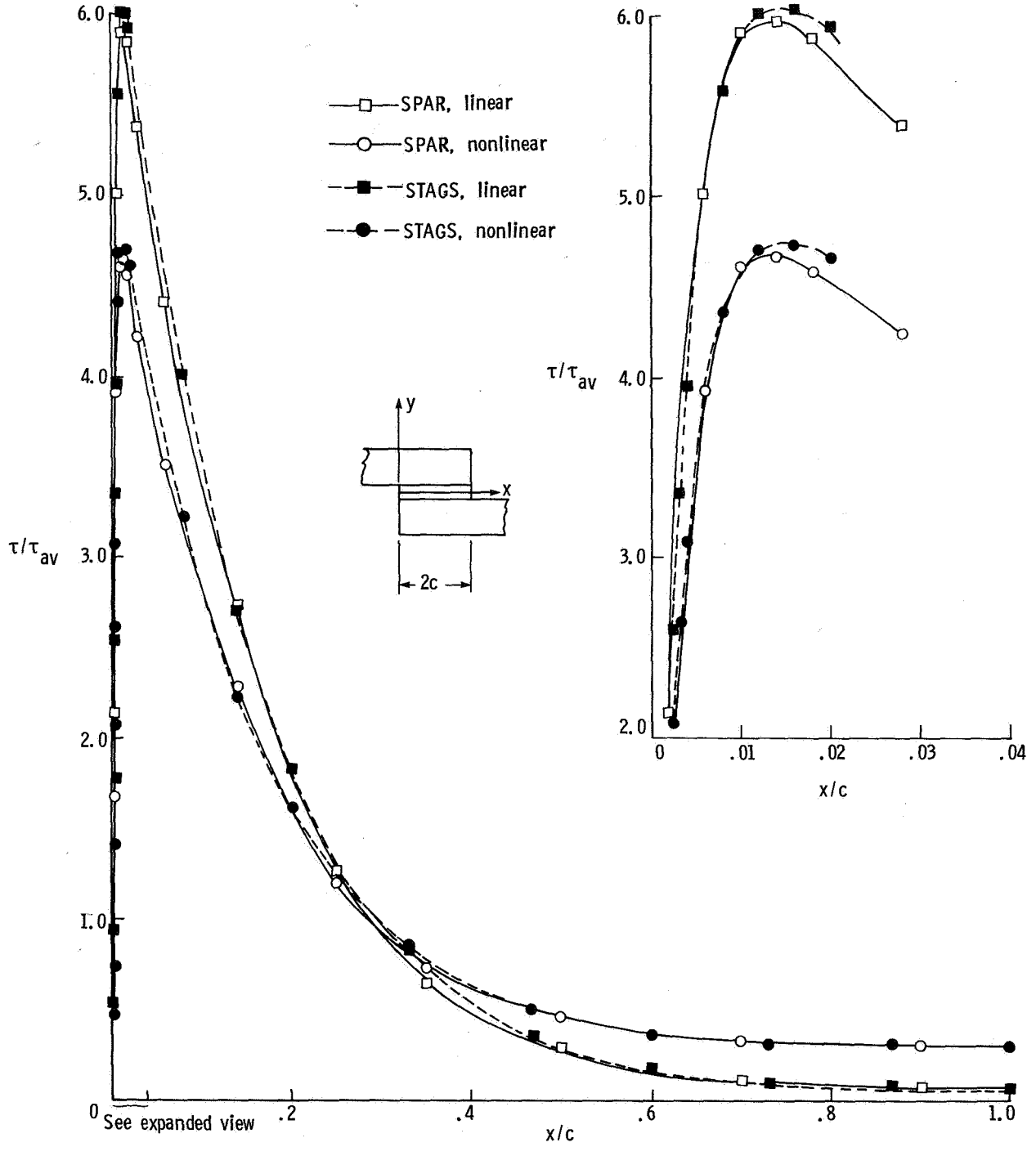

Figure 10.- Comparison of shear stress distributions along center line of adhesive given by finite-difference and finite-element analyses. T = 175 kN/m (1000 lbf/in.); τ_{av} = T/2c.

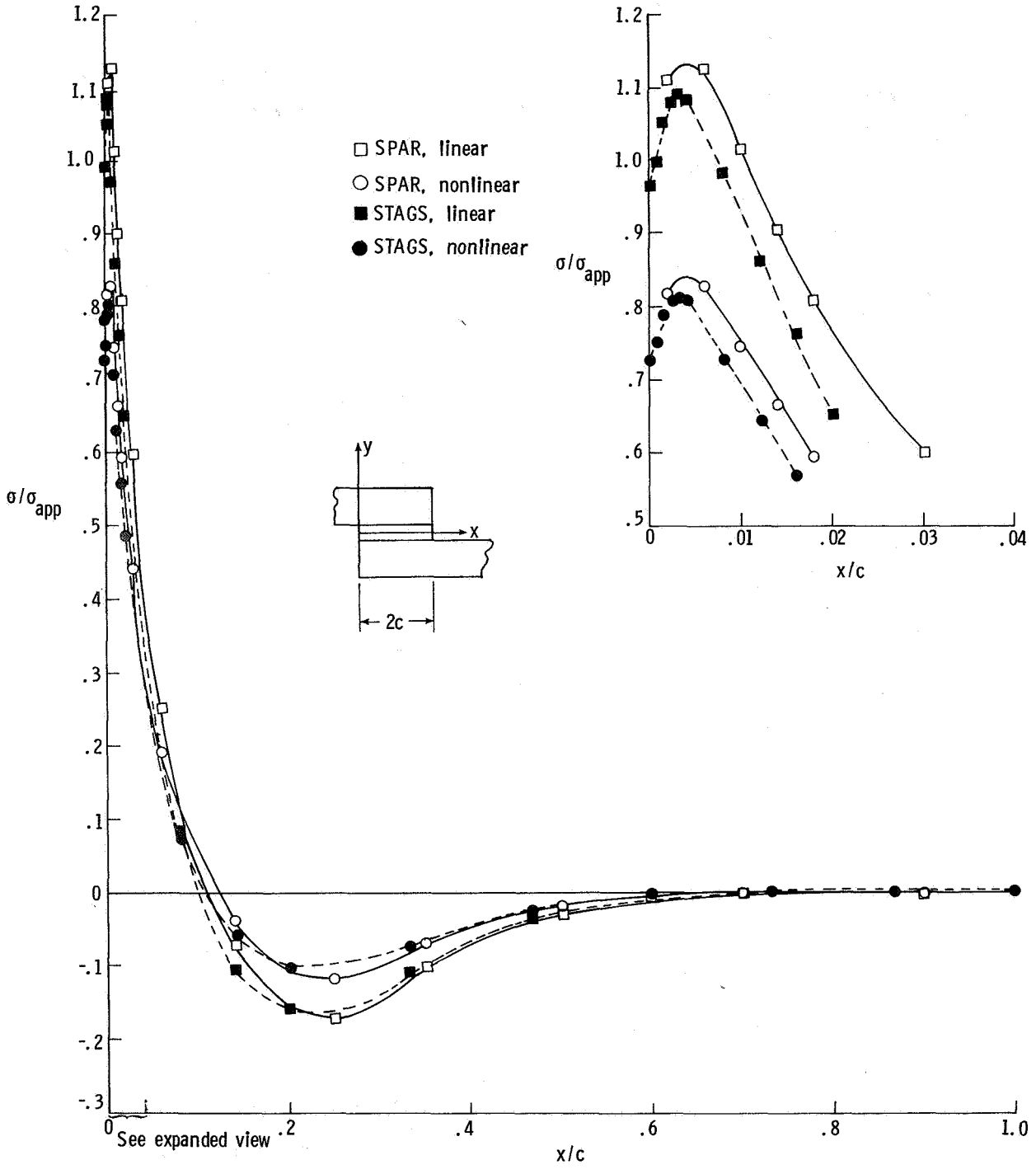

Figure 11.- Comparison of peel stress distributions along center line of adhesive given by finite-difference and finite-element analyses. T = 175 kN/m (1000 lbf/in.); $\sigma_{app} = T/t$.

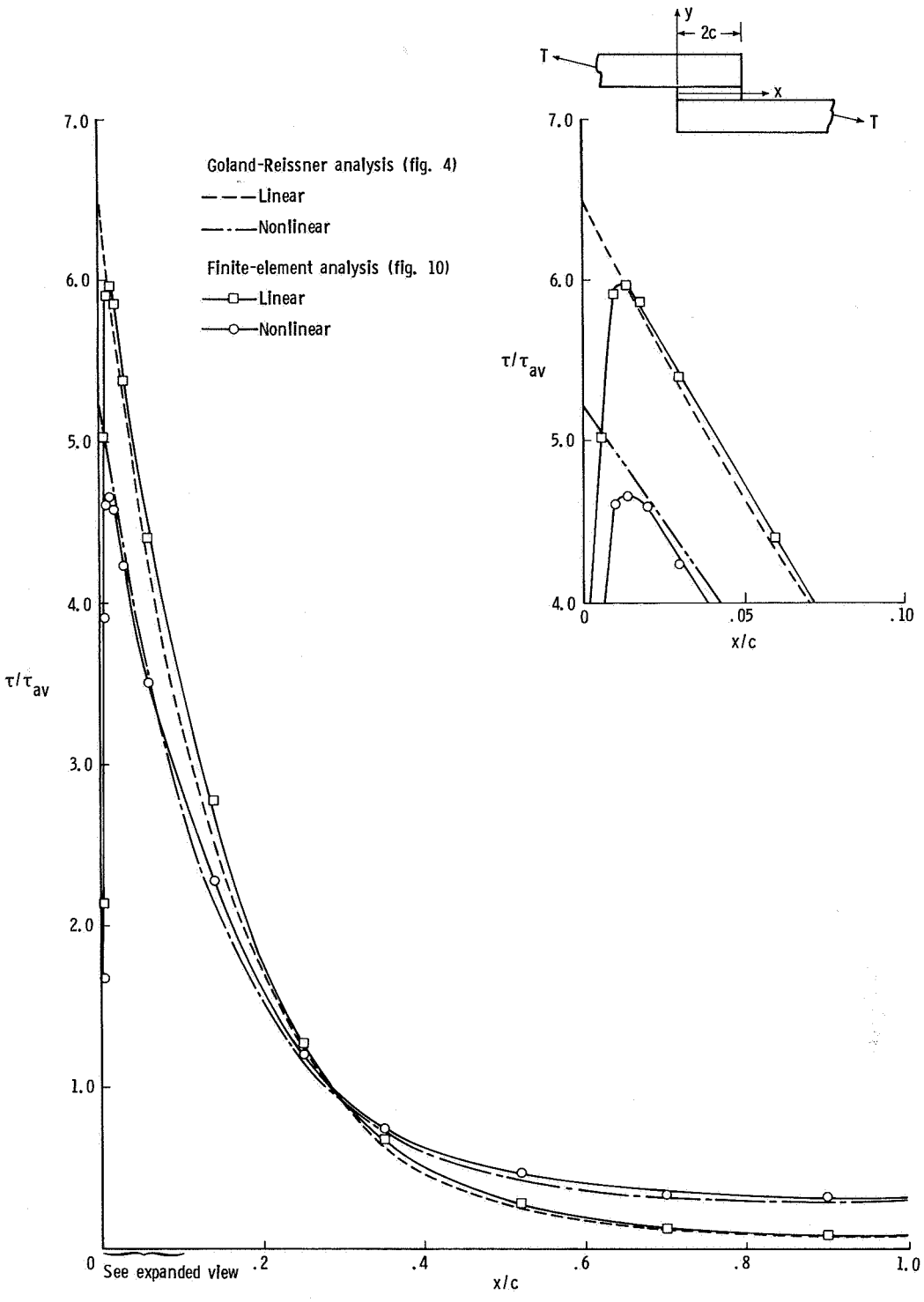

Figure 12.- Comparison of shear stress distributions along center line of adhesive given by Goland-Reissner analysis and finite-element analysis. T = 175 kN/m (1000 lbf/in.); $\tau_{av} = T/2c$.

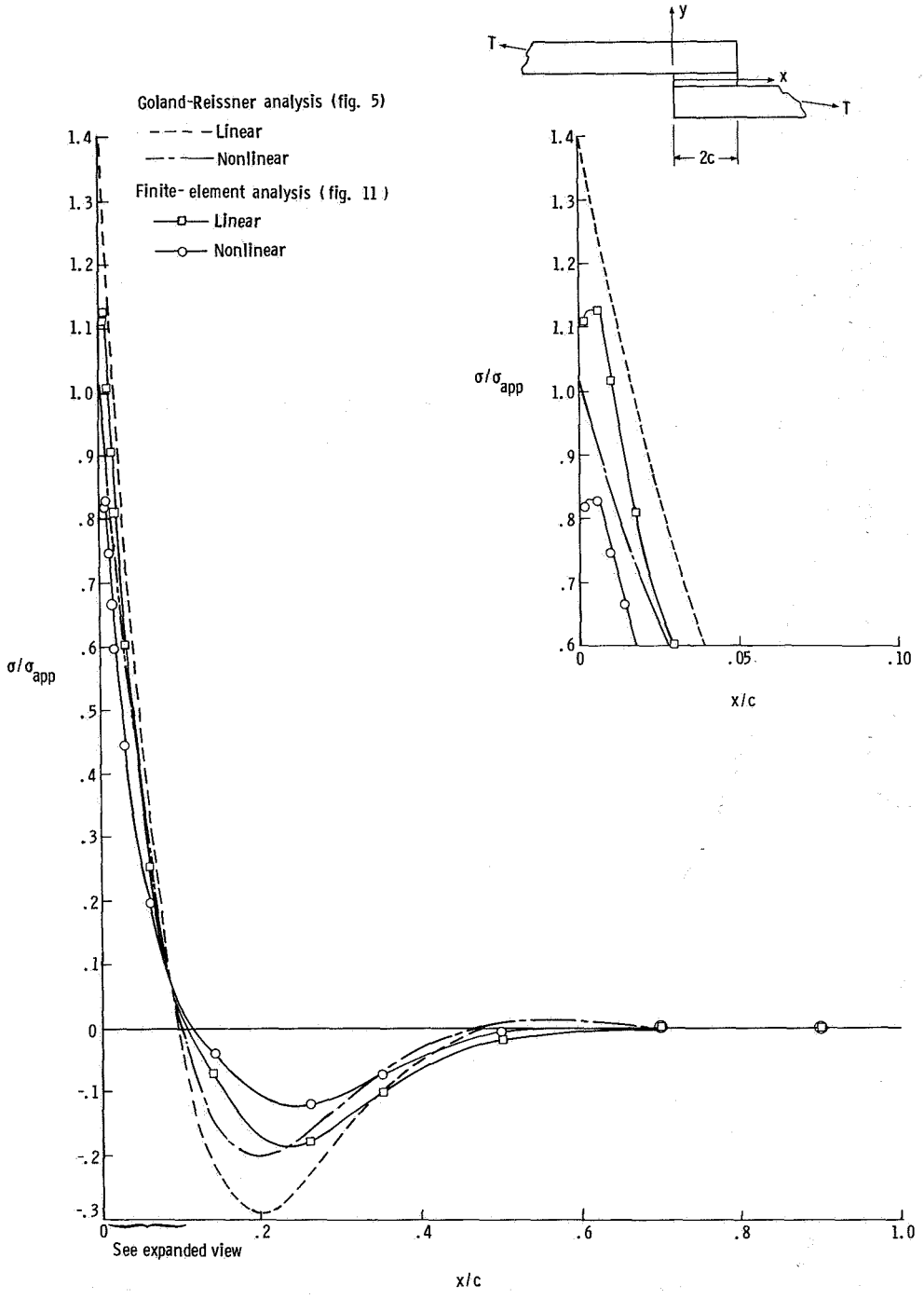

Figure 13.- Comparison of peel stress distributions along center line of adhesive given by Goland-Reissner analysis and finite-element analysis. T = 175 kN/m (1000 lbf/in.); σ_{app} = T/t.

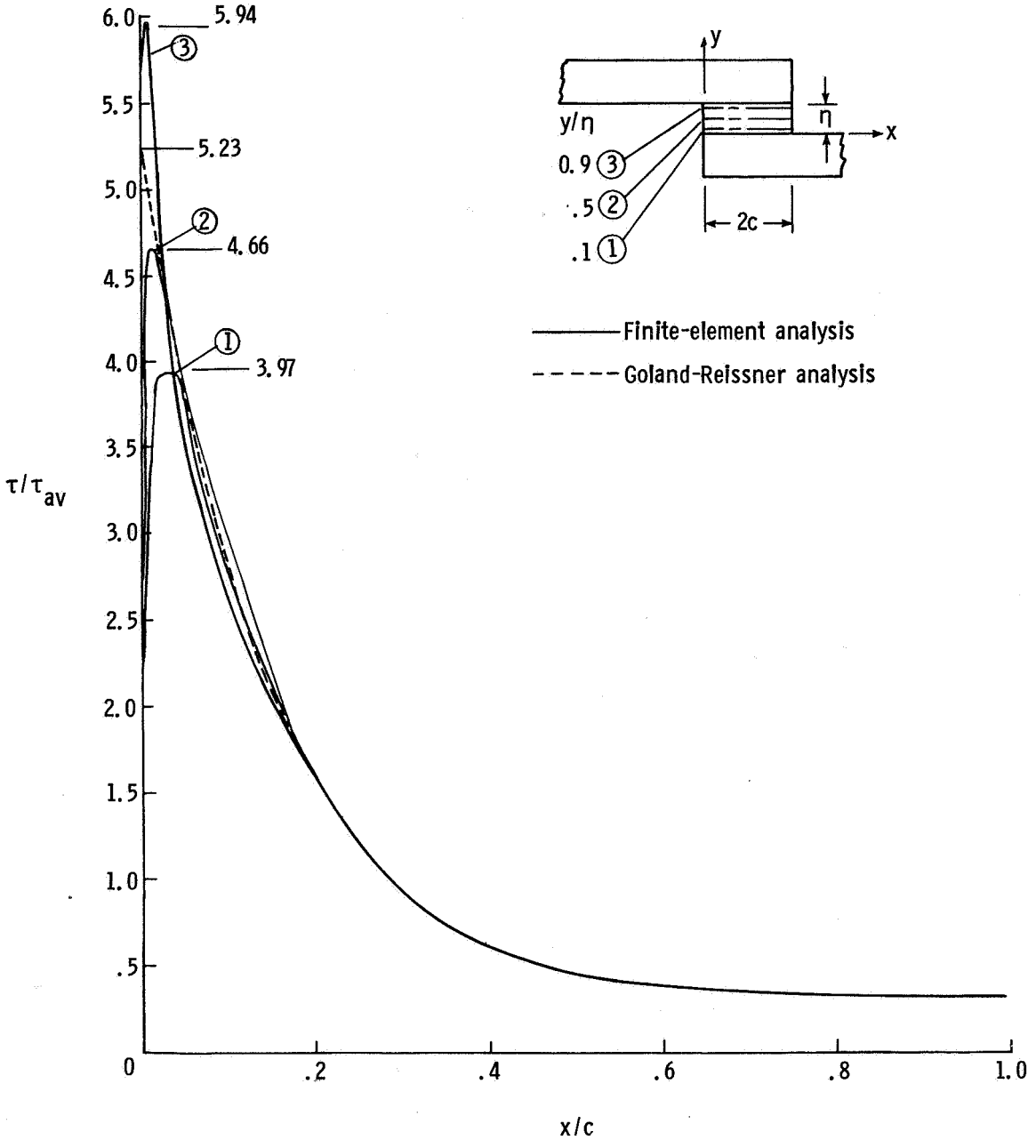

Figure 14.- Shear stress distributions at various positions through adhesive. T = 175 kN/m (1000 lbf/in.); $\tau_{av} = T/2c$.

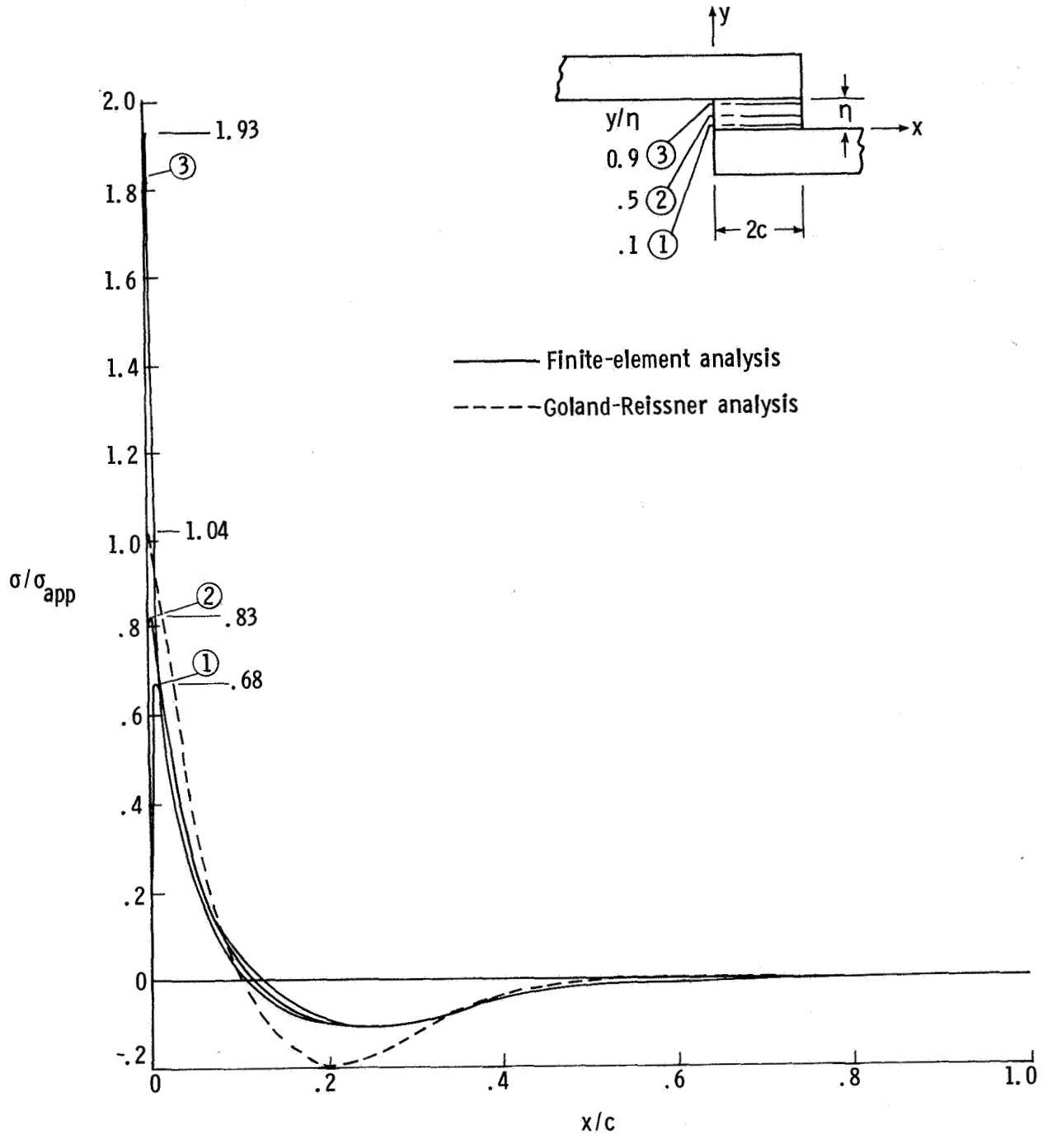

Figure 15.- Peel stress distributions at various positions through adhesive. T = 175 kN/m (1000 lbf/in.); $\sigma_{app} = T/t$.

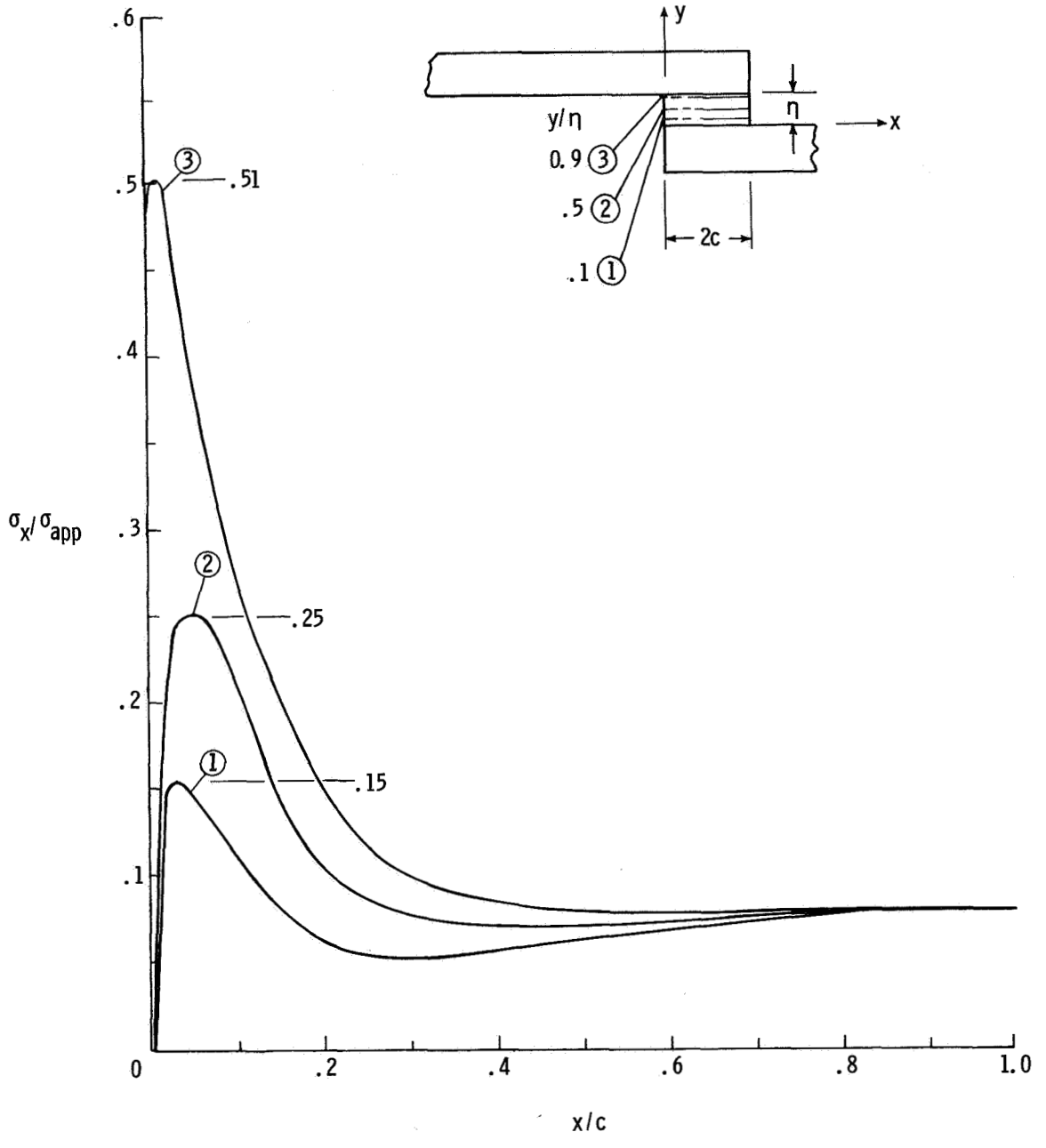

Figure 16.- In-plane stress distributions at various positions through adhesive. T = 175 kN/m (1000 lbf/in.); $\sigma_{app} = T/t$.

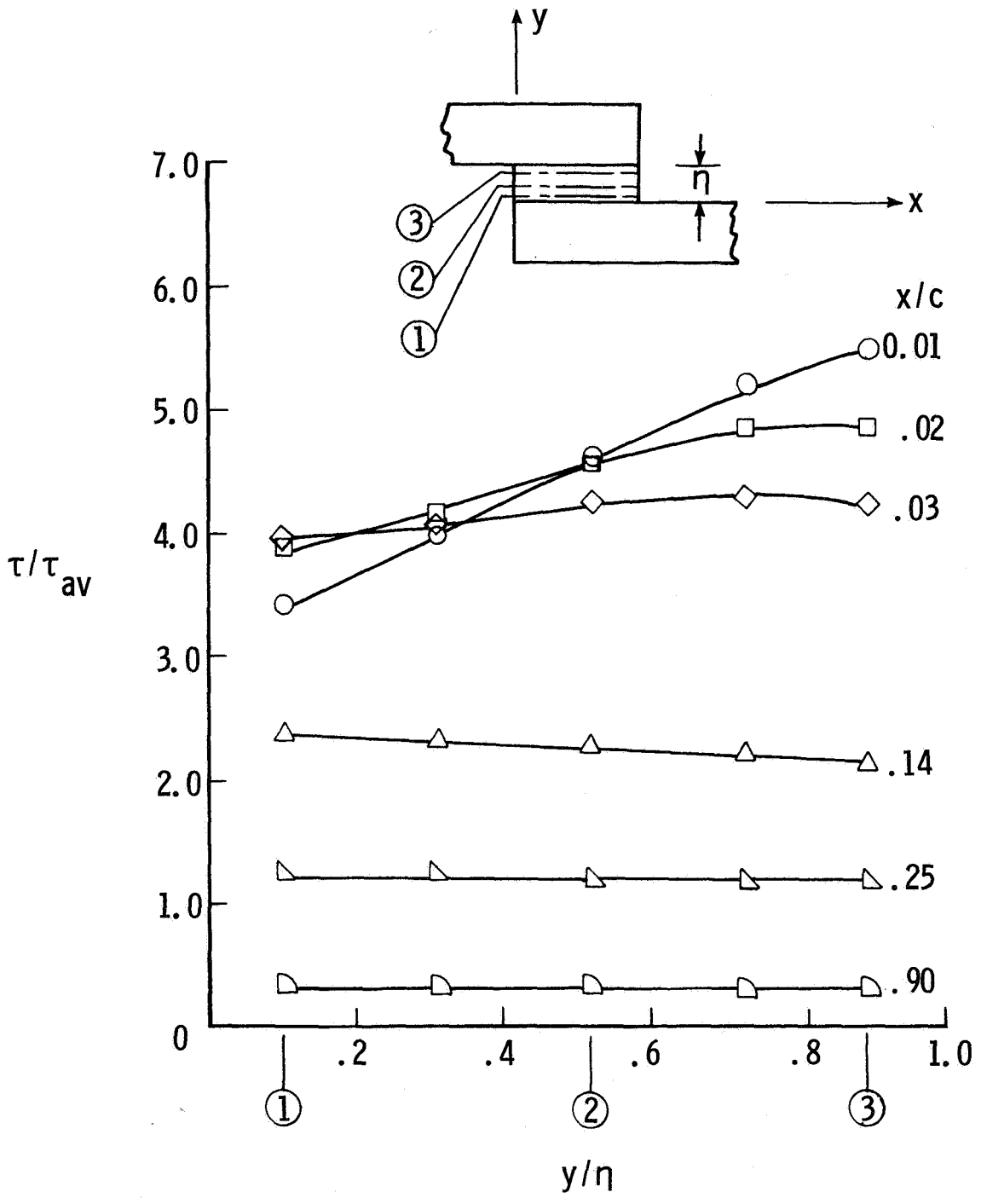

Figure 17.- Shear stress distributions through adhesive. T = 175 kN/m (1000 lbf/in.); τ_{av} = T/2c.

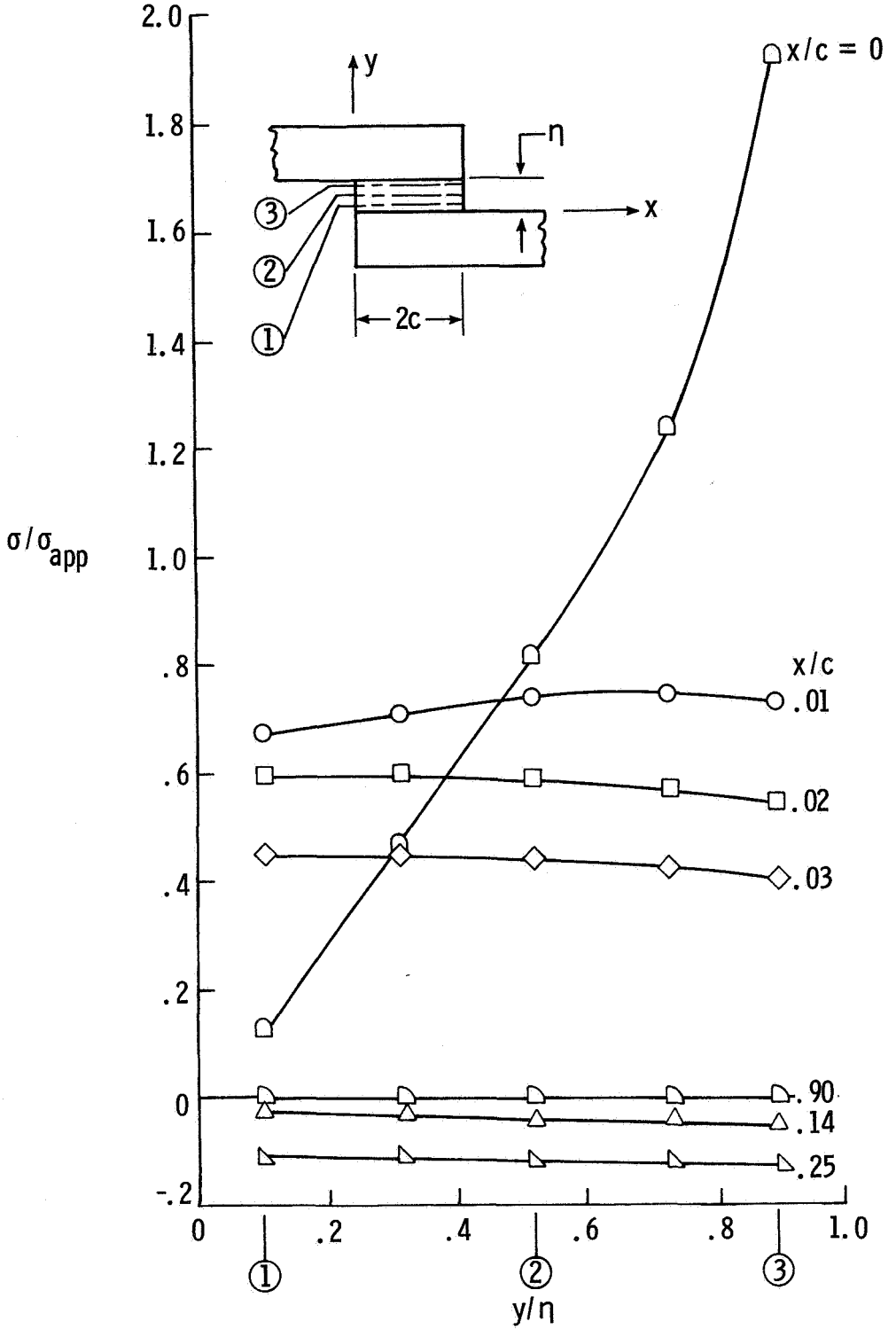

Figure 18.- Peel stress distribution through adhesive. T = 175 kN/m (1000 lbf/in.); $\sigma_{app} = T/t$.

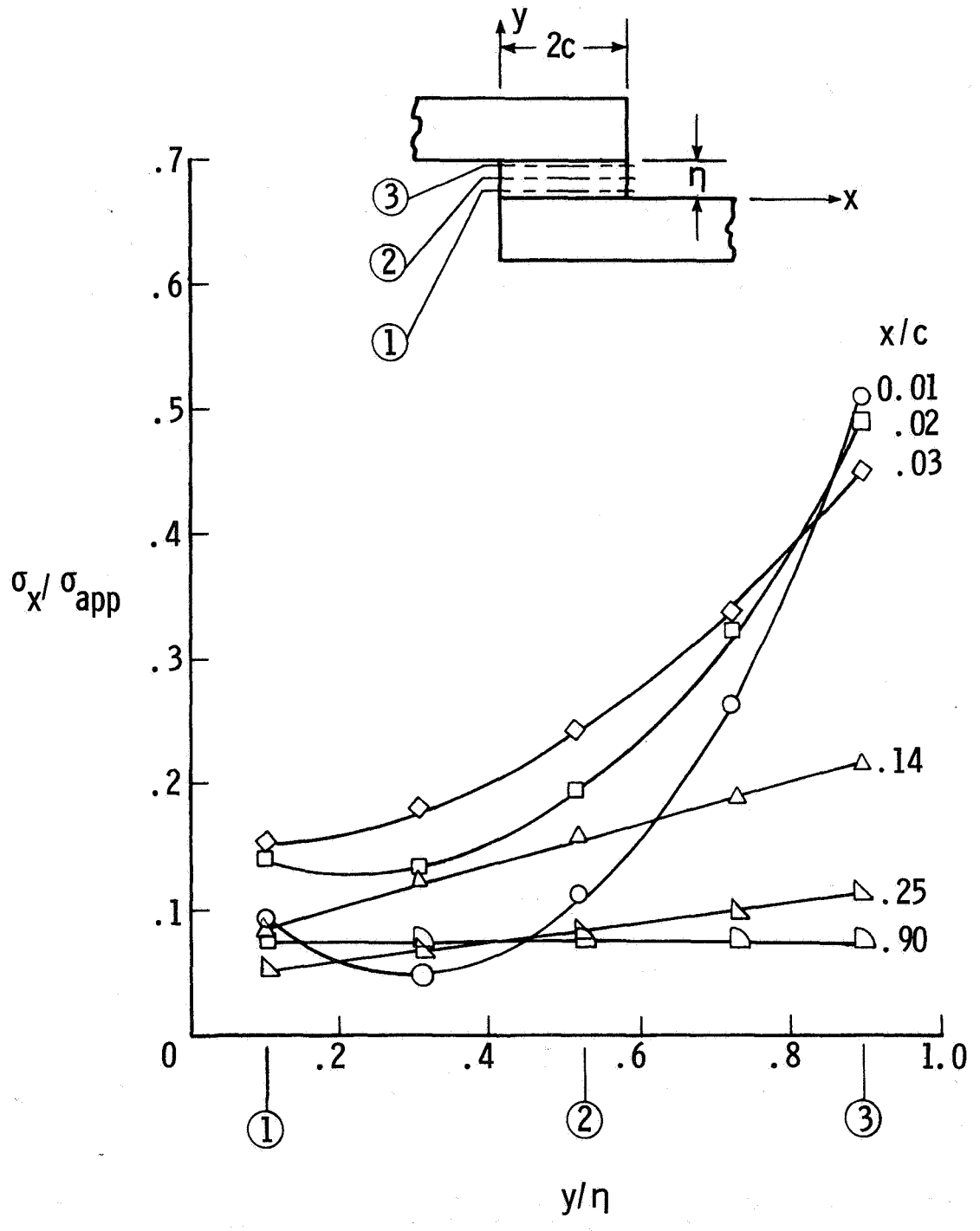

Figure 19.- In-plane stress distributions through adhesive. T = 175 kN/m (1000 lbf/in.); $\sigma_{app} = T/t$.

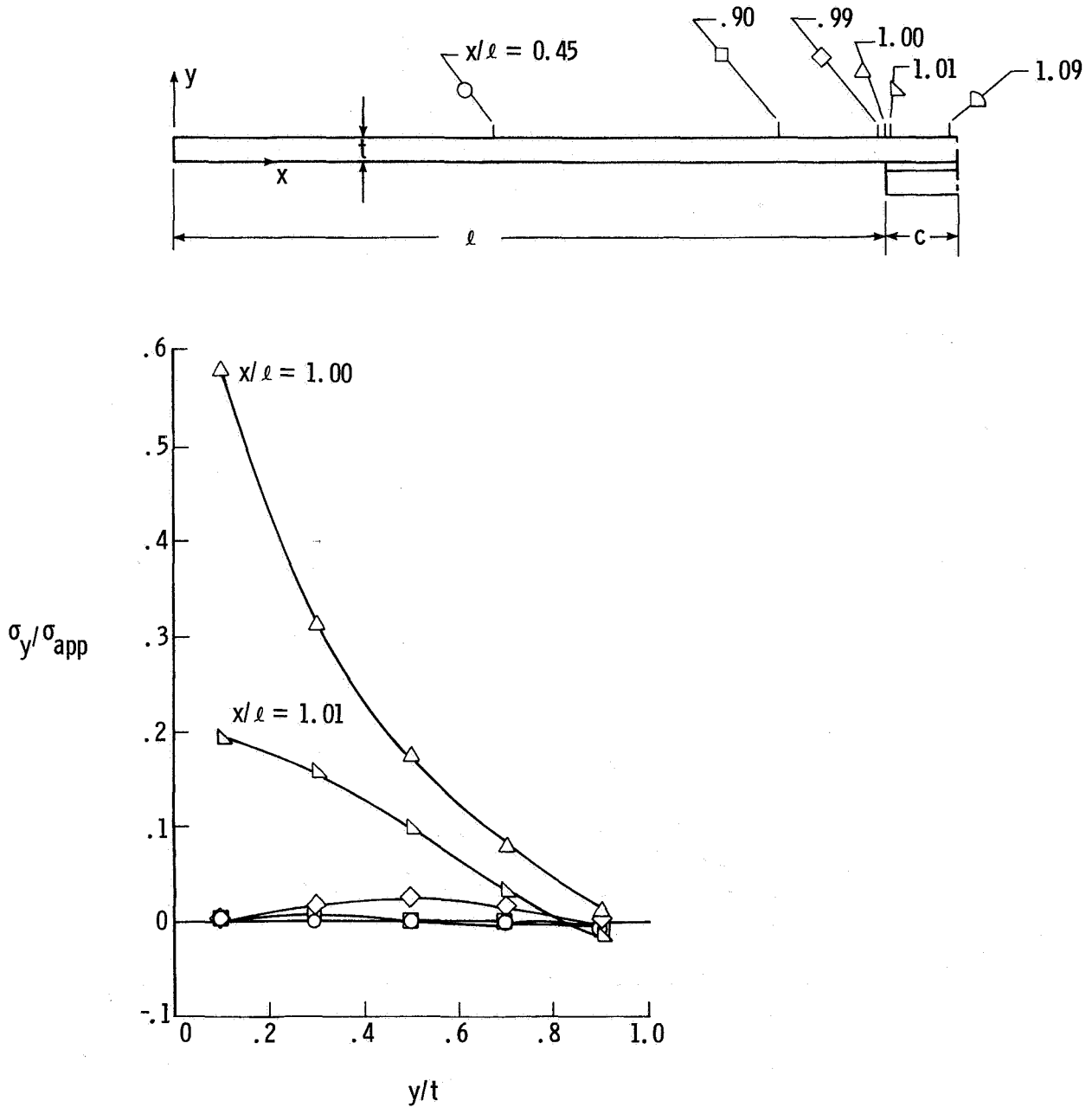

Figure 20.- Adherend transverse stress distributions at various locations. T = 175 kN/m (1000 lbf/in.); $\sigma_{app} = T/t$.

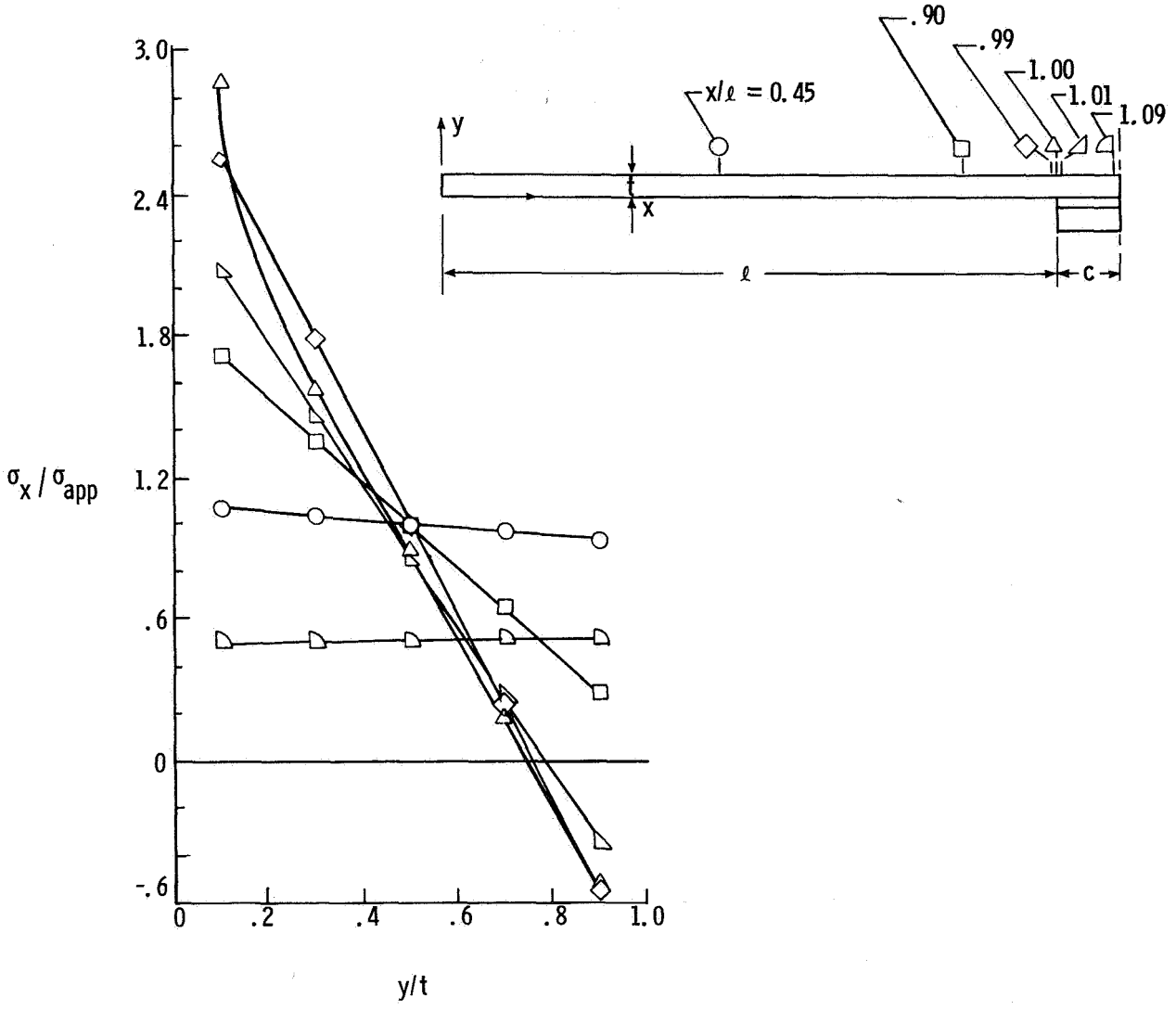

Figure 21.- Adherend axial stress distributions at various locations. T = 157 kN/m (1000 lbf/in.); σ_{app} = T/t.

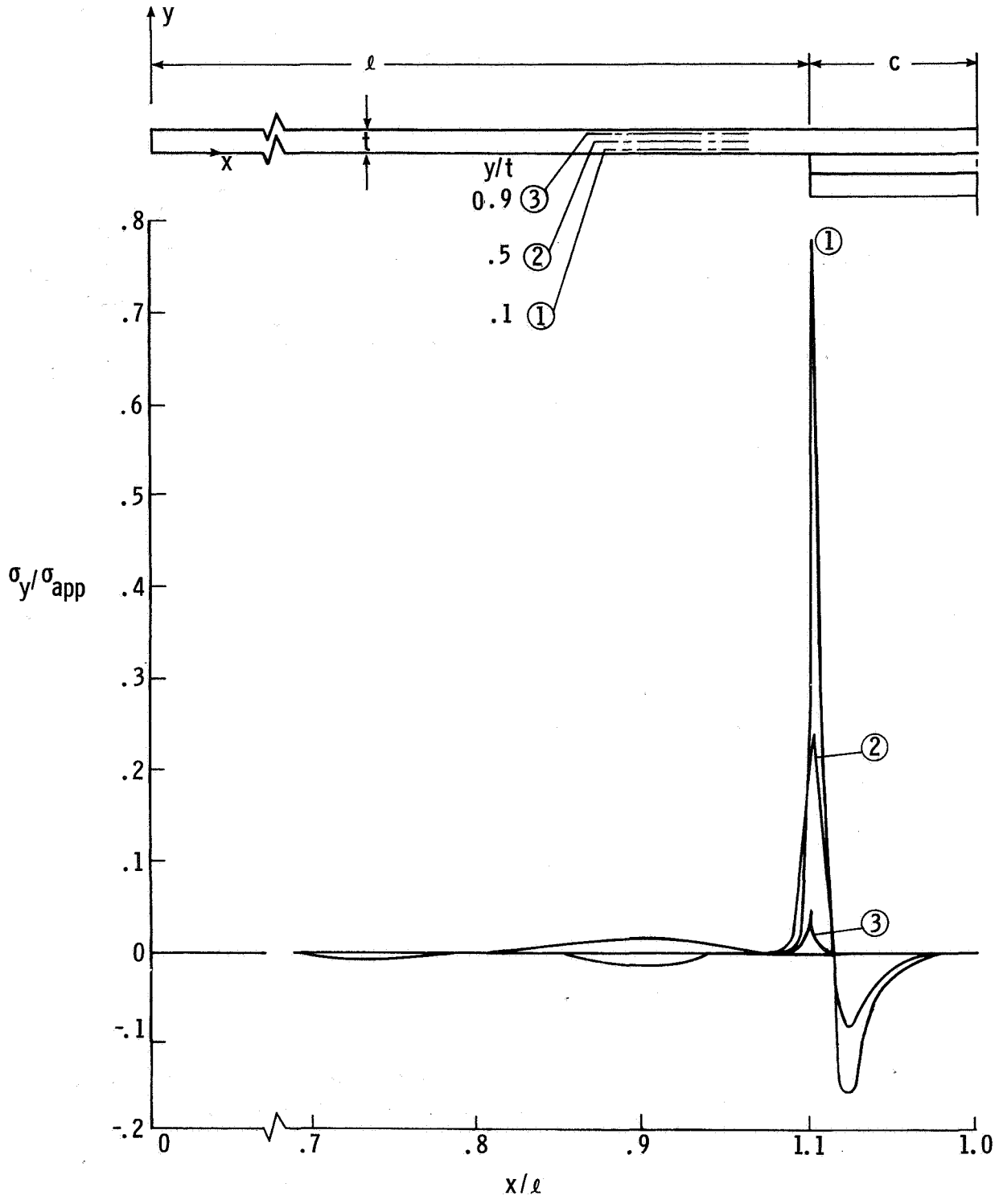

Figure 22.- Transverse stress distributions at various positions through adherend. T = 175 kN/m (1000 lbf/in.); $\sigma_{app} = T/t$.

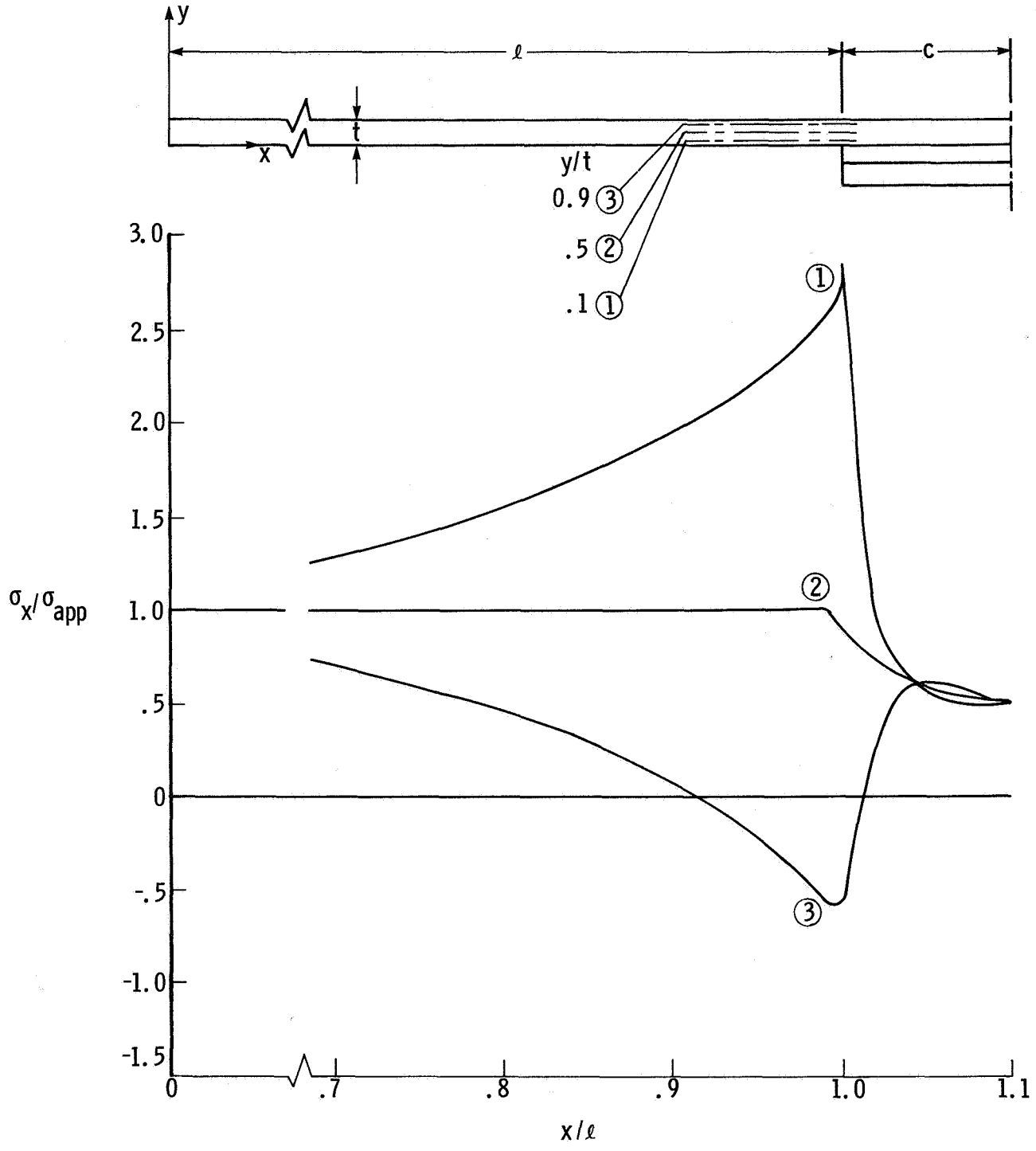

Figure 23.- Axial stress distributions at various positions through adherend. T = 175 kN/m (1000 lbf/in.); σ_{app} = T/t.

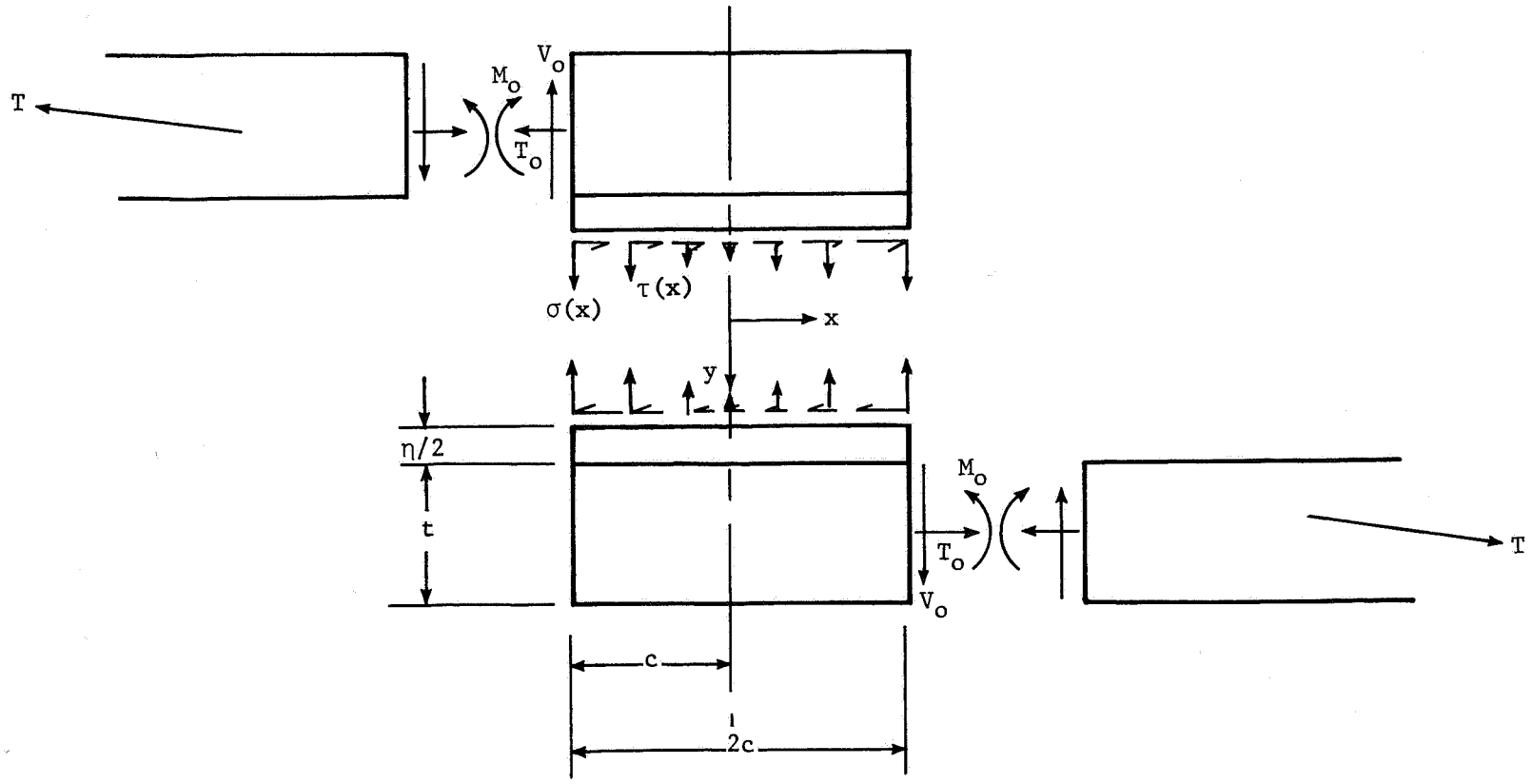

Figure 24.- Internal forces in lap region shown in positive directions.

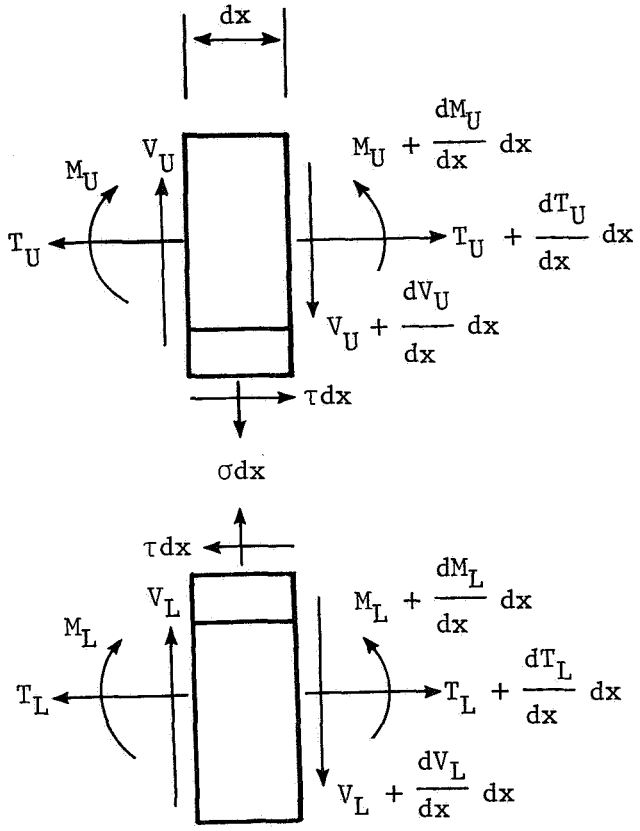

Figure 25.- Forces on differential element shown in positive direction.

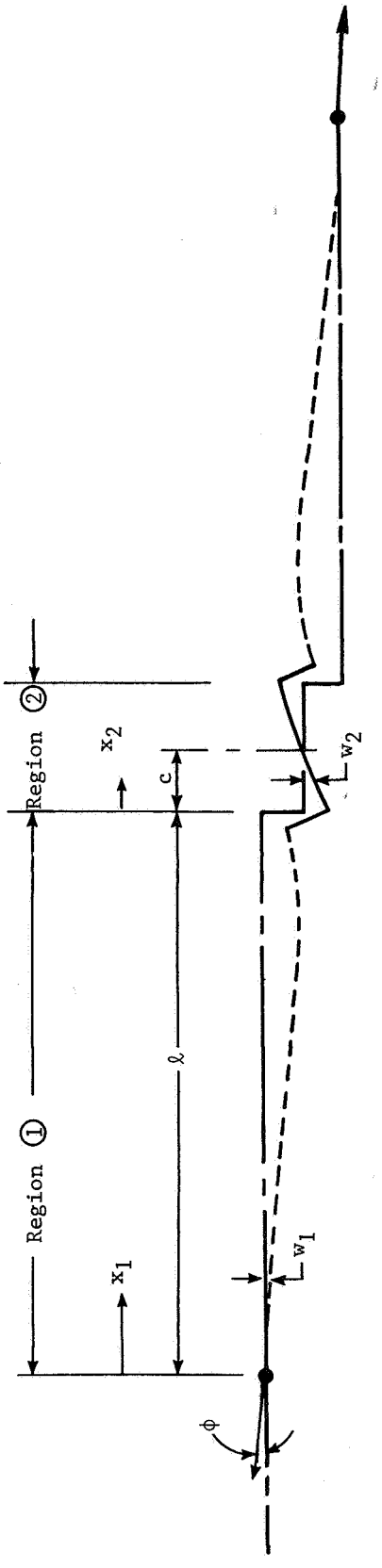

Figure 26.- Deformation of elastic axis of lap joint.

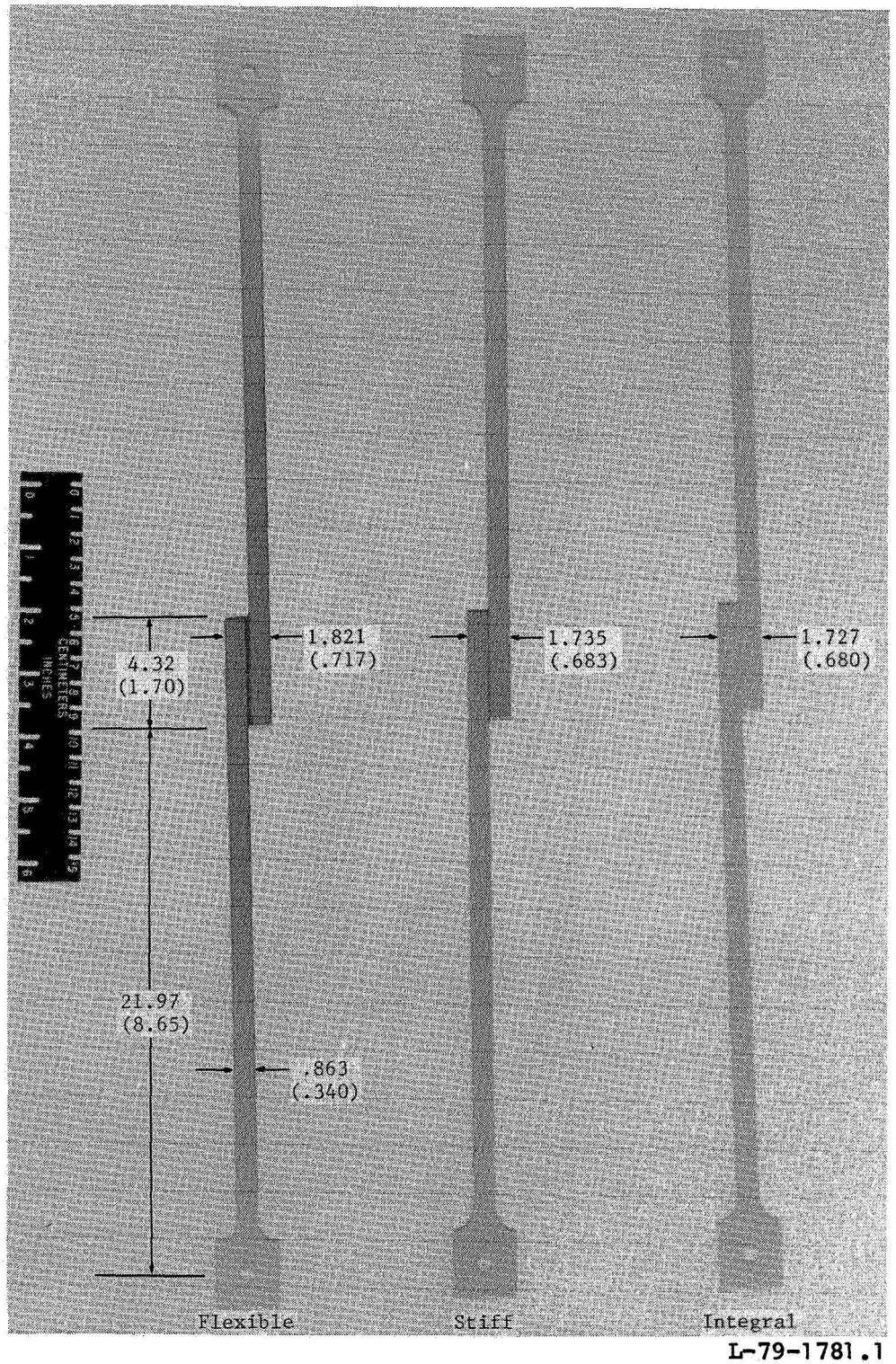

L-79-1781.1

Figure 27.- Photograph of photoelastic models. Dimensions are given in centimeters (inches).

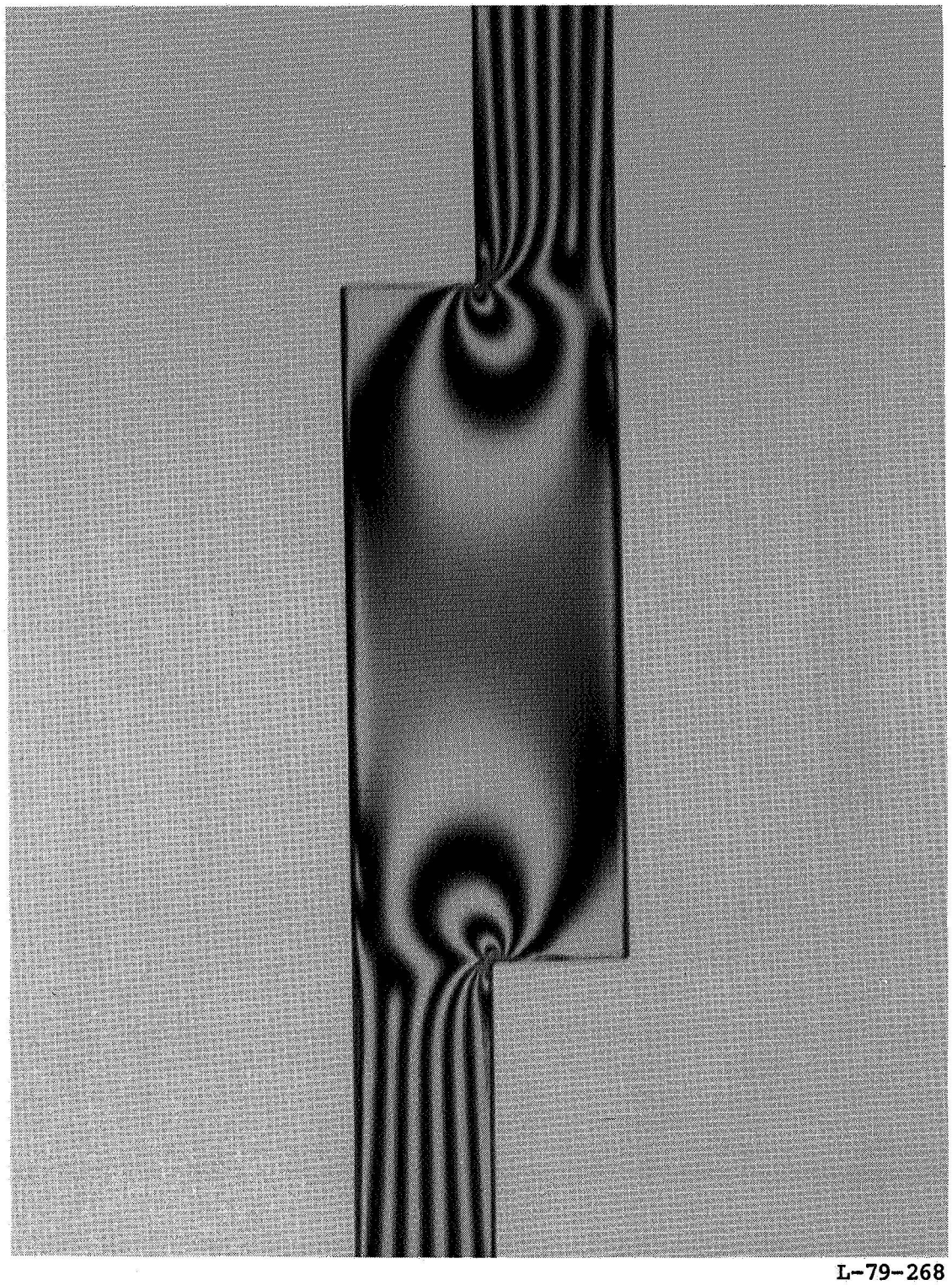

L-79-268

(a) Integral model.

Figure 28.- Photoelastic studies of single-lap models.

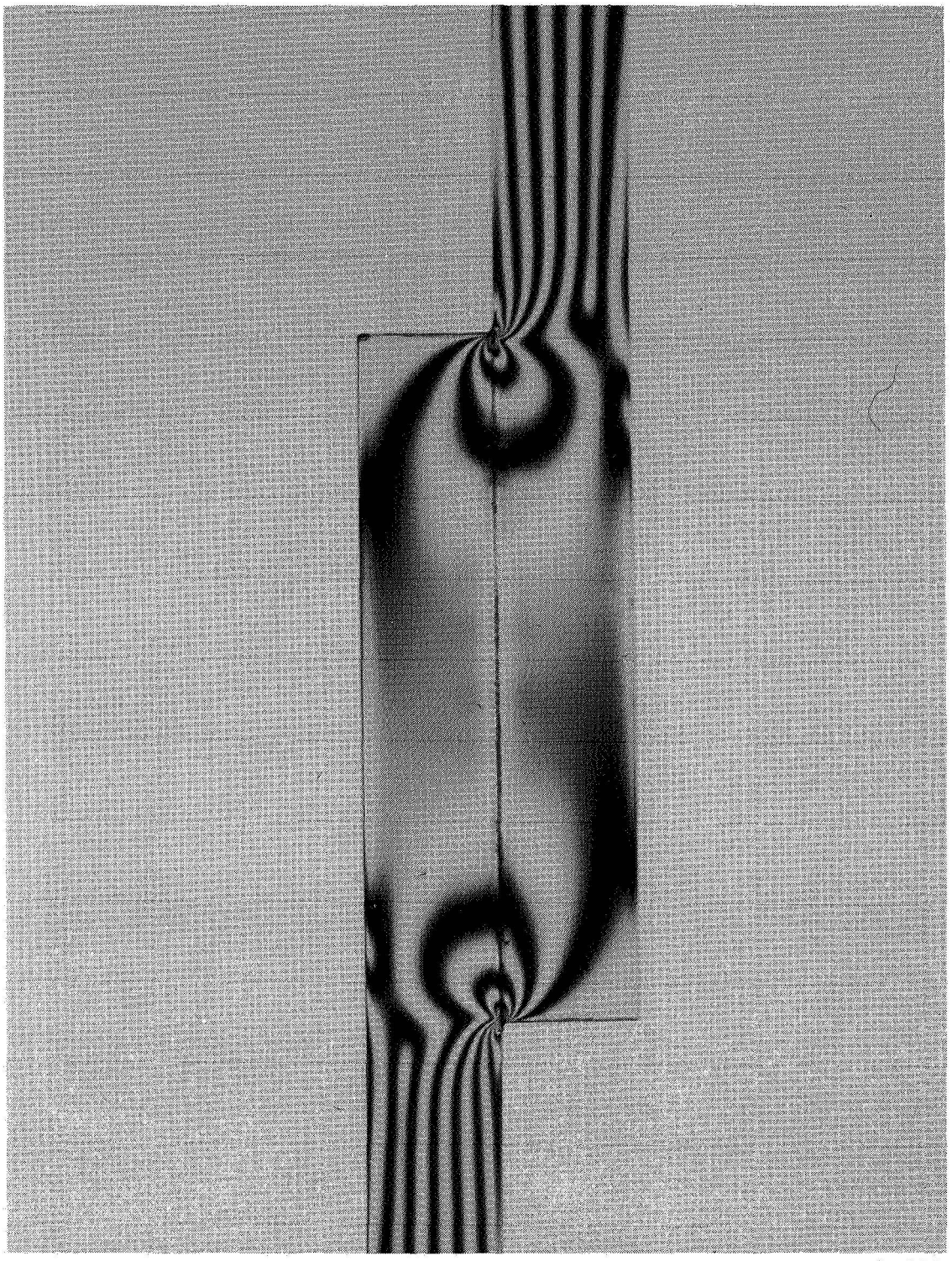

L-79-269

(b) Stiff adhesive model.

Figure 28.- Continued.

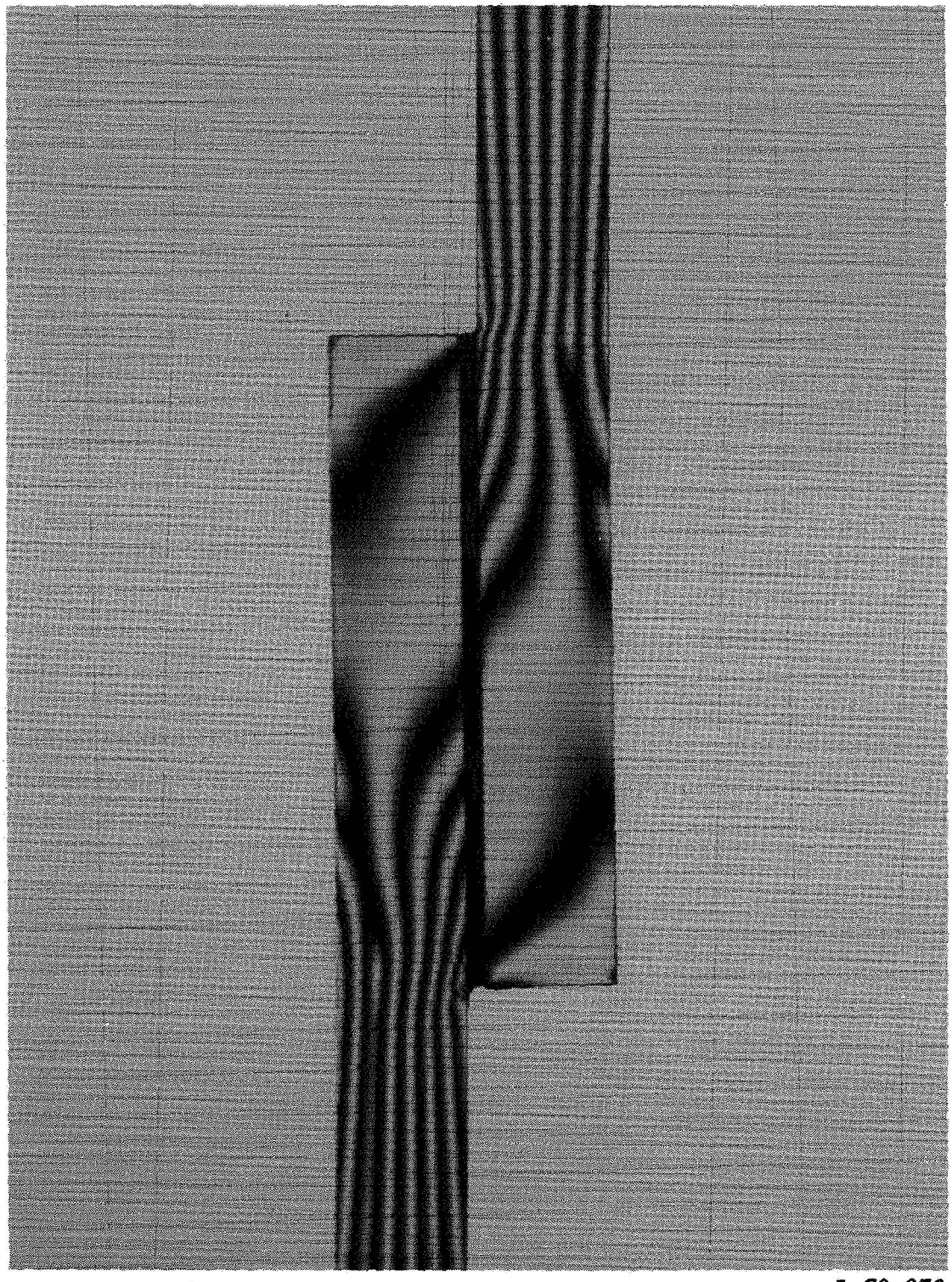

L-79-270

(c) Flexible adhesive model.

Figure 28.- Concluded.

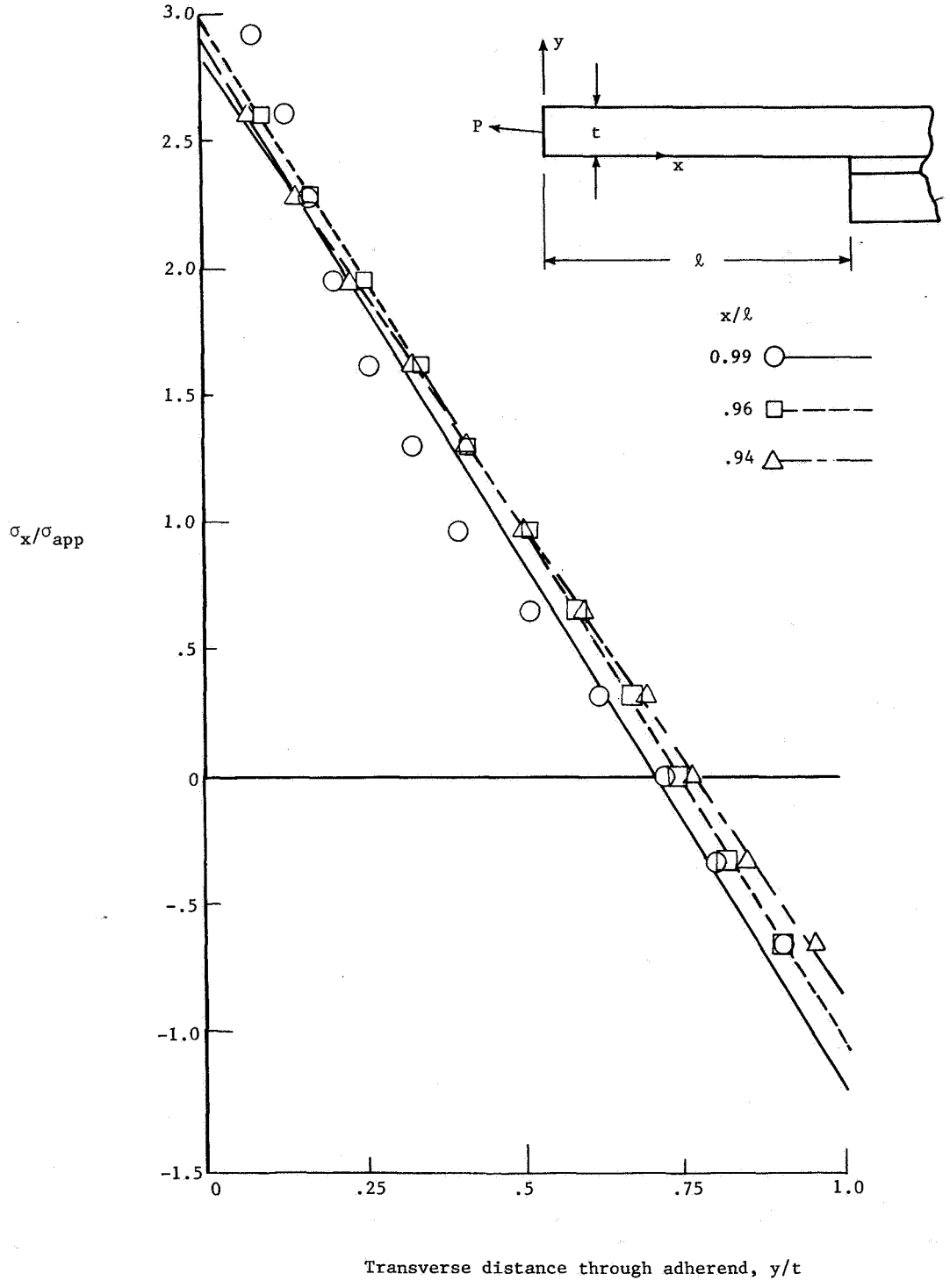

Figure 29.- Photoelastic measurement of adherend stress distribution near overlap. Stiff adhesive model; $\sigma_{app} = P/a$; P = 133 N (30 lbf); a = 0.32 cm^2 (0.05 in^2); ℓ = 22.0 cm (8.65 in.); c = 4.32 cm (1.70 in.); t = 0.86 cm (0.34 in.).

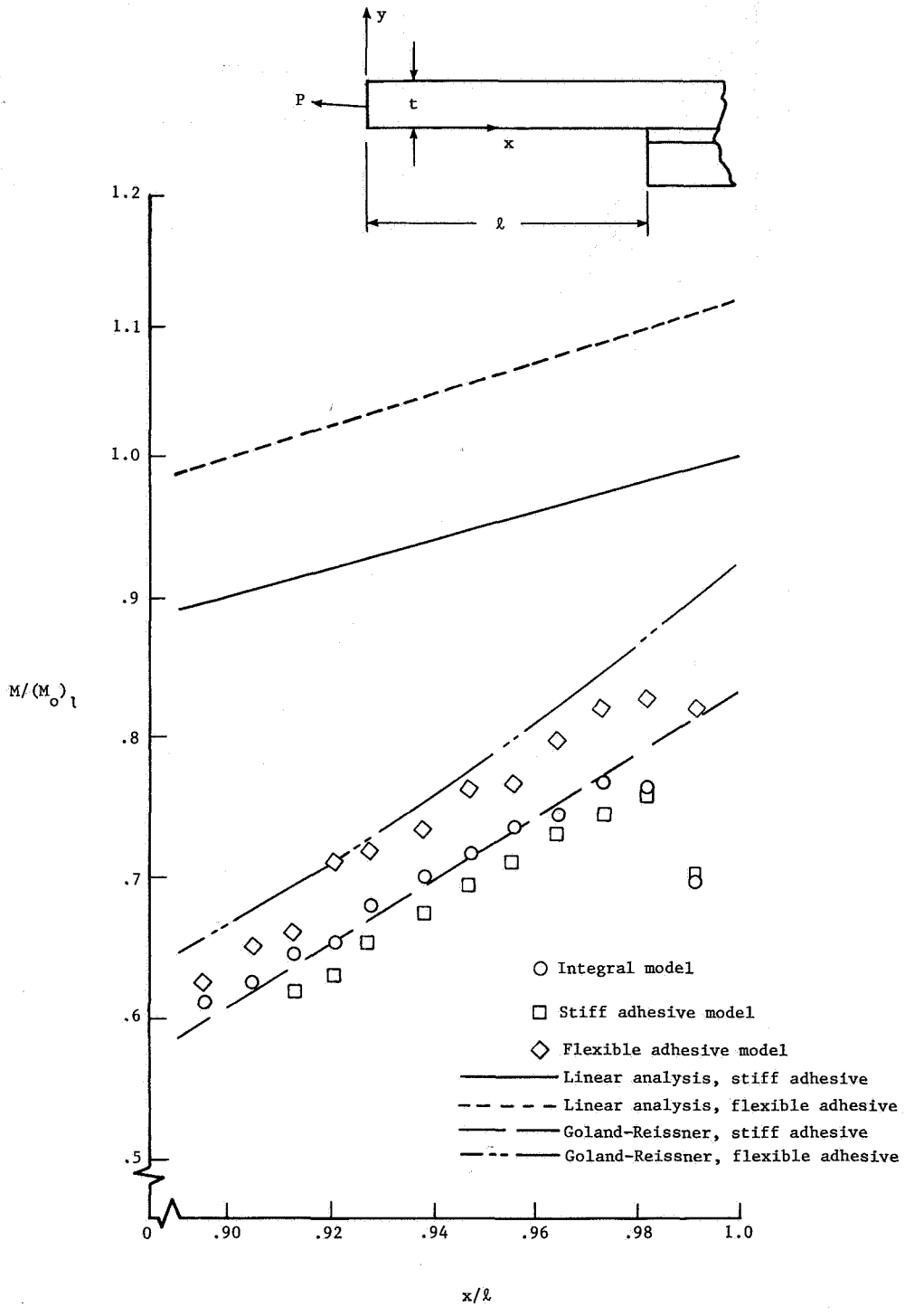

Figure 30.- Moment distribution along adherend near overlap. T = 133 N (30 lbf).